Palaeogeography, Palaeoclimatology, Palaeoecology 668 (2025) 112891

Contents lists available at ScienceDirect

Palaeogeography, Palaeoclimatology, Palaeoecology

journal homepage: www.elsevier.com/locate/palaeo

Calcareous plankton and shallow-water benthic biocalcifiers: Resilience and extinction across the Cenomanian-Turonian Oceanic Anoxic Event 2

Maria Rose Petrizzo [a,*], Mariano Parente [b], Francesca Falzoni [c], Cinzia Bottini [a], Gianluca Frijia [d], Thomas Steuber [e], Elisabetta Erba [a]

[a] Dipartimento di Scienze della Terra "Ardito Desio", Università degli Studi di Milano, Milano, Italy
[b] Dipartimento di Scienze della Terra, dell'Ambiente e delle Risorse, Università di Napoli Federico II, Napoli, Italy
[c] Istituto di Geologia Ambientale e Geoingegneria (IGAG), Consiglio Nazionale delle Ricerche, Milano, Italy
[d] Dipartimento di Fisica e Scienze della Terra, Università degli Studi di Ferrara, Ferrara, Italy
[e] Earth Science Department, Khalifa University of Science and Technology, Abu Dhabi, United Arab Emirates

ARTICLE INFO

Keywords:
Extinction and resilience
Hyperthermal
Planktonic foraminifera
Calcareous nannoplankton
Larger benthic foraminifera
Rudists

ABSTRACT

Oceanic Anoxic Event 2 (OAE 2), spanning the Cenomanian/Turonian boundary (93.9 Ma), was an episode of major perturbation of the global carbon cycle. Its geochemical signature is a synchronous positive $\delta^{13}C$ excursion in both carbonates and organic matter that resulted from the net burial of large amounts of organic carbon in deep-sea and hemipelagic settings.

Causes for OAE 2 are still the subject of investigations; however, several studies postulate that massive submarine volcanic activity emitted greenhouse gases and provided biolimiting metals in marine ecosystems, leading to the onset of the Cenomanian-Turonian thermal maximum and to the enhancement of ocean fertility. Ocean temperature, sea-surface stratification, nutrient availability, and carbonate ion saturation were subject to variations during OAE 2 that resulted in fluctuations in diversity abundance and calcification of species.

We analyzed the record of the main biocalcifiers of pelagic-hemipelagic settings (planktonic foraminifera and calcareous nannofossils) and of low-latitude carbonate platforms (larger benthic foraminifera and rudist bivalves) by looking at well-dated sections. Carbon isotope stratigraphy allowed precise correlation from shallow to deep water and tied the biotic response to the record of geochemical proxies of paleoenvironmental changes. The main extinction event, severely affecting the shallow-water benthic biocalcifiers and to a minor extent the calcareous plankton, occurred within and after the Plenus Cold Event. Fluctuations in surface seawater temperature and extreme warming were probably the main cause of extinction, with contributions from decreased seawater carbonate saturation and disruption of ocean stratification. Overall, calcareous plankton fared much better, showing a greater resilience than carbonate-platform biocalcifiers to paleoenvironmental perturbations across OAE 2.

Editor name: Professor L Angiolini.

1. Introduction

The latest Cenomanian-earliest Turonian Oceanic Anoxic Event 2 (OAE 2, e.g., Schlanger and Jenkyns, 1976; Scholle and Arthur, 1980; Schlanger et al., 1987) represents the last prominent global Oceanic Anoxic Event. OAE 2 is associated to a positive $\delta^{13}C$ excursion in both carbonates and organic matter that is globally correlatable (e.g., Tsikos et al., 2004; Voigt et al., 2006, 2008; Jenkyns, 2010; Wendler, 2013; Jenkyns et al., 2017; Robinson et al., 2017; Gale et al., 2019). The isotopic excursion likely resulted from the net burial of large amounts of organic matter in deep-sea and hemipelagic settings (e.g., Kuroda and Ohkouchi, 2006; Trabucho Alexandre et al., 2010 and references therein). However, anoxic conditions were not pervasive during this interval in shallow marine environments (Gertsch et al., 2010).

Several hypotheses have been presented to account for the increase in the global rate of organic-carbon burial during OAE 2, including increase in the delivery of weathering-derived nutrients to the oceans (Frijia and Parente, 2008; Blättler et al., 2011; Monteiro et al., 2012;

* Corresponding author.
E-mail address: mrose.petrizzo@unimi.it (M.R. Petrizzo).

https://doi.org/10.1016/j.palaeo.2025.112891
Received 29 October 2024; Received in revised form 28 February 2025; Accepted 6 March 2025
Available online 10 March 2025

Pogge von Strandmann et al., 2013), sea-level rise that promoted the increase in the flux of recycled nutrients to the oceans (Erbacher et al., 2005; Bjerrum et al., 2006), incursion of oxygen minimum zones onto the continental shelf (Schlanger and Jenkyns, 1976; Arthur et al., 1987; Gavrilov et al., 2013), changes in the cycling of major nutrients (Mort et al., 2007; Adams et al., 2010; Higgins et al., 2012), input of volcanically derived nutrients to the oceans (Kerr, 1998; Larson and Erba, 1999; Leckie et al., 2002; Erba, 2004; Turgeon and Creaser, 2008; Du Vivier et al., 2014; Jenkyns et al., 2017), changes in ocean circulation (MacLeod et al., 2008; Martin et al., 2012; Zheng et al., 2013), and a combination of the above changes coinciding with an increase in seasonality after a long eccentricity (2.4 Myr) cycle minimum (Mitchell et al., 2008; Batenburg et al., 2016).

OAE 2 was probably triggered by submarine volcanic activity (i.e., emplacement of the Caribbean, High Arctic, and part of the Kerguelen Plateau Large Igneous Provinces) that injected large amounts of CO_2, sulfides and trace metals into the ocean and atmosphere leading to the enhancement of ocean fertility (e.g., Larson, 1991; Kuypers et al., 2002; Leckie et al., 2002; Jenkyns, 2003; Erba, 2004; Pancost et al., 2004; Kuroda et al., 2007; Turgeon and Creaser, 2008; Barclay et al., 2010; Trabucho Alexandre et al., 2010; Zheng et al., 2013; Du Vivier et al., 2014; Scaife et al., 2017; Schröder-Adams et al., 2019; Jones et al., 2021, 2023).

The Cenomanian-Turonian boundary interval is also accompanied by warming of the ocean (e.g., Jenkyns et al., 1994; Clarke and Jenkyns, 1999; Bice et al., 2003; Voigt et al., 2004; Friedrich et al., 2012). Surface-ocean temperatures exceeded 35 °C at low latitudes (Wilson et al., 2002; Forster et al., 2007; Moriya et al., 2007; Friedrich et al., 2012; MacLeod et al., 2013; O'Brien et al., 2017), and equator-to-pole sea surface temperature gradients were reduced to about 5 °C in surface and bottom waters (Huber et al., 2002; Linnert et al., 2014; O'Brien et al., 2017; Huber et al., 2018).

Regionally, the warming during the OAE 2 interval was briefly interrupted by a cooling event known as the Plenus Cold Event (PCE; after Gale and Christensen, 1996) that has been attributed to a decrease in atmospheric pCO_2 forced by the widespread burial of organic carbon (Arthur et al., 1988; Kuypers et al., 1999; Voigt et al., 2006; Barclay et al., 2010; Sinninghe Damsté et al., 2010; Jarvis et al., 2011; van Bentum et al., 2012; Gale et al., 2019; O'Connor et al., 2020). Cooling in the early part of OAE 2 has been first documented in the Anglo-Paris and Vocontian Basins by the incursion of a Boreal macrofossil fauna found to coincide with two $\delta^{18}O$ shifts of bulk carbonates toward higher values in the Shakespeare Cliff section at Dover, England (Gale and Christensen, 1996), subsequently confirmed in other sections of both basins (Voigt et al., 2004, 2006; Jarvis et al., 2011; Jenkyns et al., 2017; Gale et al., 2019; O'Connor et al., 2020; Jeans et al., 2021). Occurrence of Boreal macrofossils coinciding with $\delta^{18}O$ shifts as well as with changes in the Nd-isotope signatures and in other geochemical elements were also documented in other sections of the Anglo-Paris Basin, suggesting coeval changes in ocean circulation patterns and increased oxygenation at the sea-floor (Jefferies, 1962, 1963; Hart et al., 1991; Morel, 1998; Paul et al., 1999; Tsikos et al., 2004; Voigt et al., 2004, 2006; Zheng et al., 2013; Jenkyns et al., 2017; Clarkson et al., 2018; Desmares et al., 2020; O'Connor et al., 2020; Jeans et al., 2021). The cooling event has been reported in other localities across the Tethyan margins, North to central Atlantic, and Western Interior Seaway (WIS) based on faunal assemblages (Friedrich et al., 2006; Voigt et al., 2006; van Helmond et al., 2016; Eldrett et al., 2017), foraminiferal coiling direction (Desmares et al., 2016), $\delta^{18}O$ values (Morel, 1998; Caron et al., 2006; Keller et al., 2008; Desmares et al., 2016; Kuhnt et al., 2017; Kalanat et al., 2018), and TEX_{86} measurements (Forster et al., 2007; Sinninghe Damsté et al., 2010).

The environmental perturbations associated to OAE 2 certainly influenced the evolutionary history of planktonic (e.g., Erbacher et al., 1996; Leckie et al., 2002; Erba, 2004; Pearce et al., 2009) and benthic (Parente et al., 2008; Steuber et al., 2023; Křížová et al., 2024) biocalcifiers. However, after decades of studies on OAE 2, a synthesis on the combined marine shallow- and deep-water biotic records of the event is still missing. The main aim of this paper is to fill this gap by producing a detailed dataset of biotic changes (extinctions and originations) across the OAE 2 interval for the main groups of marine biocalcifiers of pelagic-hemipelagic settings (planktonic foraminifera and calcareous nannofossils) and of low latitude carbonate platforms (larger benthic foraminifera and rudist bivalves).

We use carbon isotope stratigraphy to establish a common time framework from basins to platforms and to tie precisely the record of bioevents with the record of geochemical proxies of paleoenvironmental changes. Timing and selectivity across different groups of organisms are then used to evaluate the potential causes of extinction.

Finally, we try to answer the main question raised by our dataset: why larger benthic foraminifera and rudists experienced a mass extinction across the OAE 2 interval while planktonic foraminifera and calcareous nannoplankton were much more resilient?

2. Materials and methods

In this paper, we use published and some new data from three well-known hemipelagic-pelagic sections (Rock Canyon, Pueblo, USA, 38°16′56"N, 104°43′39"W; Gun Gardens, Eastbourne, UK, 50°44′12.001"N, 0°14'53.998"E; Clot Chevalier, France, 43°59′32.02"N, 6°24′14.27″E) to illustrate the biotic changes in planktonic foraminifera and calcareous nannoplankton across OAE 2 (Fig. 1). New data only concern the calcareous nannofossil biostratigraphy of the Eastbourne section. Specifically, a total of 138 samples (from 0 to 26.9 m, Fig. 2) were analyzed. Smear slides were prepared using the standard technique described by Bown and Young (1998) and were studied under a Leitz Laborlux polarizing light microscope at 1250×.

For carbonate platform environments we present data on Larger Benthic Foraminifera (LBF) and rudist bivalves. For LBF we use published data from the Raia del Pedale section (southern Italy, 40°13′57.09"N, 15°26′48.49″E) and from the Lusitanian Carbonate Platform (Portugal). For rudist bivalves we use data from the Lusitanian Carbonate Platform and review literature data from the northern and southern margins of Tethys and the Americas (Fig. 1).

Carbon isotope stratigraphy, described in subchapter 2.1, is used to establish a high-resolution correlation between the hemipelagic-pelagic and the carbonate platform sections analyzed in this study and to compare the record of biotic changes with the record of geochemical proxies for surface seawater temperature, pCO_2, silicate weathering intensity, sea-floor anoxia and volcanism.

The detailed description of the hemipelagic-pelagic and carbonate platform sections and of the published and new data on the calcareous plankton and shallow-water benthic taxa are presented in subchapters 2.2 and 2.3, respectively, for each stratigraphic section examined in this study.

2.1. Definition of OAE 2 and nomenclature of the carbon isotope excursion

OAE 2 was originally defined on the basis of the widespread occurrence of broadly coeval organic-carbon rich deposits across the Cenomanian-Turonian boundary interval (Schlanger and Jenkyns, 1976). A few years later it was documented that the event was associated with a positive carbon isotope excursion (CIE) close to the Cenomanian/Turonian boundary recorded on a global scale (Scholle and Arthur, 1980). Detailed studies based on integrated stratigraphy documented that the onset and termination of the deposition of organic-rich sediments were not synchronous in different basins, due to local paleoenvironmental conditions interfering with global paleoenvironmental perturbations (Tsikos et al., 2004; Grosheny et al., 2017). At the same time, it was realised that the CIE was much more reliable than the distribution of organic-rich sediments as a tool to define the onset and

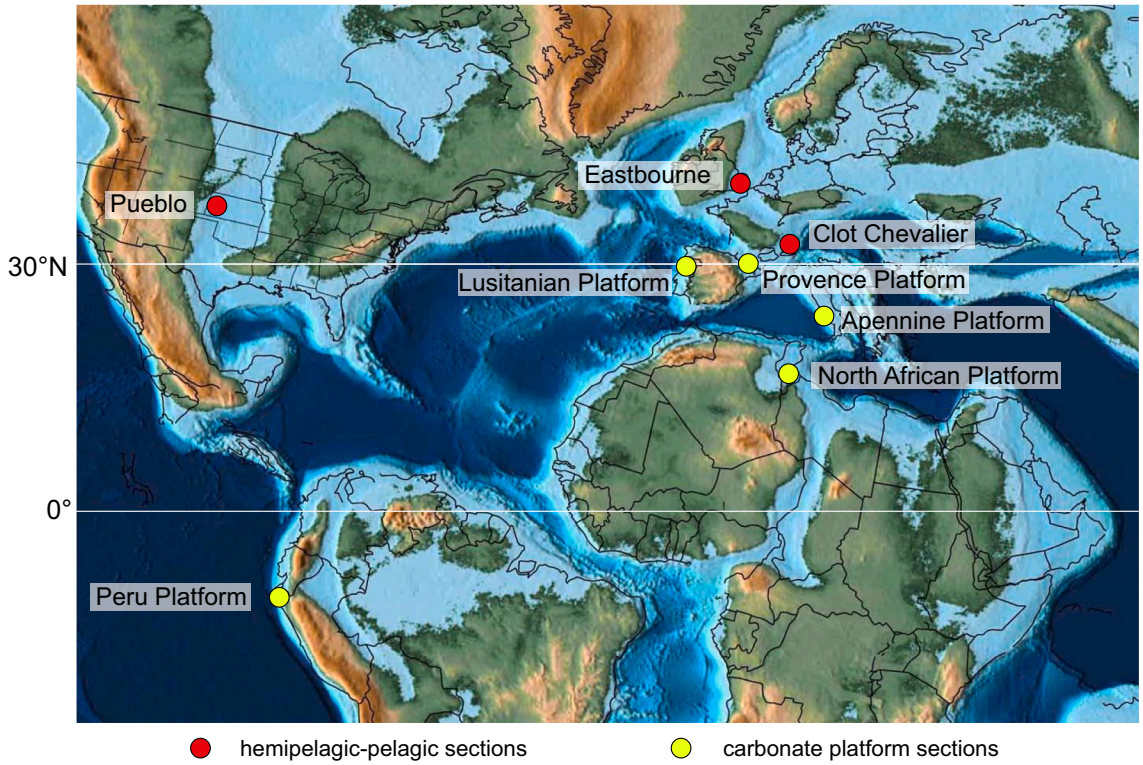

Fig. 1. Paleogeographic reconstruction (Scotese, 2016) for the Cenomanian/Turonian boundary (93.6 Ma) with location of the stratigraphic sections analyzed and mentioned in this study.

termination of the event and to correlate records of different basins and across different facies and latitudes (see for instance Tsikos et al., 2004). Following this chemostratigraphic approach, OAE 2 was defined as the stratigraphic interval from the onset of the positive CIE to the point in the $\delta^{13}C$ curve where carbon isotope values start a steep decline to return to pre-excursion values (Tsikos et al., 2004). In this paper the OAE 2 interval (Fig. 2) is identified from the level of the initial positive shift into the $\delta^{13}C$ excursion (onset) through the level where $\delta^{13}C$ values begin a definite decrease from those high values (termination) according to the definition of Jarvis et al. (2011), Gambacorta et al. (2015) and Jenkyns et al. (2017). A nomenclature subdividing the OAE 2 CIE was first proposed by Pratt and Threlkeld (1984) and Pratt (1985) that interpreted peak "a" as a maximum, peak "b" as a trough and peak "c" as the entire plateau of less negative values above "b". Later Paul et al. (1999) subdivided the $\delta^{13}C$ curve of the English Chalk at Eastbourne into pre-excursion, first build-up, trough, second build-up, plateau, recovery and post-excursion (Fig. 2). A further elaboration was the identification of three positive peaks in the inorganic carbon isotope record, labelled "a" to "c" by Jarvis et al. (2006). Peak "a" represents the positive peak reached at the end of the first build-up. Peak "b" is reached at the end of the second build-up and is separated from peak "a" by the trough. Peak "c" is at the end of the plateau. Finally, a four-peaks nomenclature was introduced by Voigt et al. (2007, 2008), who labelled as peak "d" the termination of the OAE 2 CIE, which was left unlabelled by Jarvis et al. (2006, 2011) (Fig. 2). This four-peaks nomenclature is adopted in this paper (Figs. 3–7).

Estimates of the duration of OAE 2 have been obtained in different localities using a cyclostratigraphic approach. Comparisons between the different estimates are often plagued by the problem of different definitions of the stratigraphic extent of the OAE 2 CIE and particularly of its termination (see discussion in Boulila et al., 2020). In the WIS, Sageman et al. (2006) calculated a duration of 563–601 ky for the interval going from the onset of the CIE to the end of the plateau, and of 847–885 ky, if the termination of the CIE is taken at the level where $\delta^{13}C$ values return to background values. Similar durations have been obtained using radioisotopically dated bentonites (Meyers et al., 2012) and cyclostratigraphy (Jones et al., 2021) in the WIS and in other localities such as Texas (920 ± 170 ky; Eldrett et al., 2015), Tibet (820 ± 25 ky; Li et al., 2017), New Zealand (930 ± 25 ky; Gangl et al., 2019) and Paris Basin (ca 850 ky; Boulila et al., 2020).

The Plenus Cold Event (PCE: Gale and Christensen, 1996; Jarvis et al., 2011; Jenkyns et al., 2017) temporarily interrupted the supergreenhouse conditions that prevailed during much of OAE 2. It refers to a time interval of 40–200 ky (Jarvis et al., 2011; Gangl et al., 2019; Boulila et al., 2020) characterized by cooling identified based on the geochemical proxies and the fossil record (Jenkyns et al., 2017; O'Connor et al., 2020).

The series of $\delta^{18}O$ shifts toward higher values obtained on bulk carbonates (Dover: Lamolda et al., 1994; Eastbourne: Paul et al., 1999; Tsikos et al., 2004) and on macrofossil shells (Voigt et al., 2004, 2006), is associated with a $\Delta^{13}C$ (i.e., $\delta^{13}C_{carb}$–$\delta^{13}C_{org}$) drop, which reflects an atmospheric pCO_2 decrease (Jarvis et al., 2011), and coincides with the occurrence of Boreal macrofossils, suggesting synchronism between cooling and migration of Boreal species in the Anglo-Paris and Vocontian Basins (Gale and Christensen, 1996; Jenkyns et al., 2017) (Fig. 2).

In the English Chalk, the occurrence of Boreal macrofossils (e.g., the belemnite *Praeactinocamax plenus*, the bivalve *Oxytoma seminudum;* Jefferies, 1962, 1963; Gale and Christensen, 1996; Paul et al., 1999), dinoflagellate cysts (*Cyclonephelium compactum-membraniphorum*; Dodsworth, 2000; Pearce et al., 2009), and planktonic foraminifera (*Praeglobotruncana plenusiensis, Muricohedbergella kyphoma*; Falzoni and Petrizzo, 2022) correlates with increases in the $\delta^{18}O$ values (Gale and Christensen, 1996; Paul et al., 1999; Voigt et al., 2004, 2006; Jarvis et al., 2011; Gale et al., 2019; O'Connor et al., 2020), suggesting that the PCE can be separated in at least two distinct cooler intervals interrupted by a warmer episode (Jenkyns et al., 2017). Other studies distinguish three cooler intervals interrupted by two warmer episodes (Jeans et al., 2021) (Fig. 2). Because the number of cooling episodes within the PCE in

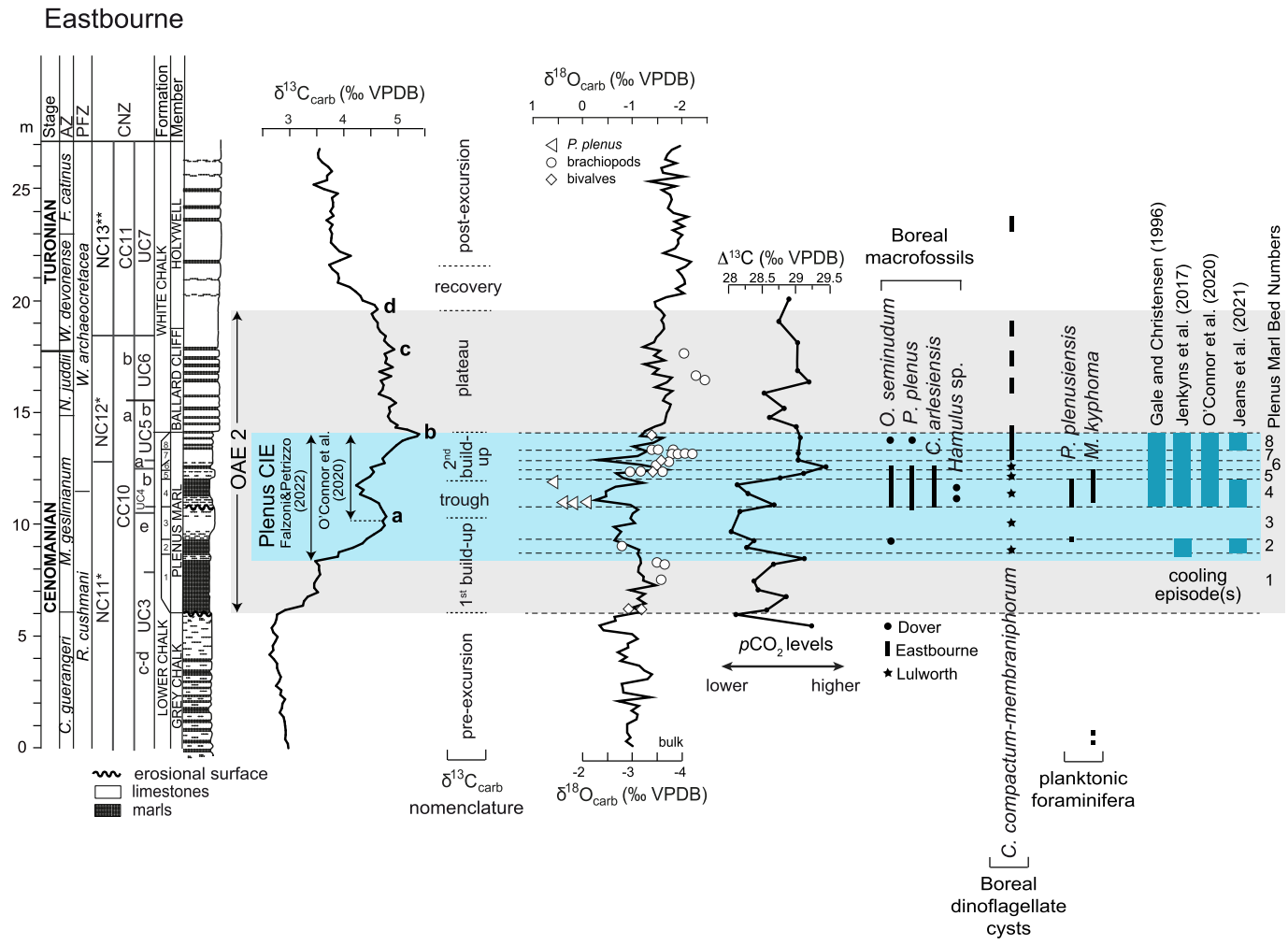

Fig. 2. Gun Gardens section, Eastbourne, SE England (Anglo-Paris Basin). Synthesis of the OAE 2 and of the Plenus Cold Event nomenclature adopted in this study, modified after Falzoni and Petrizzo (2022). Ammonite biozonation (AZ) follows Gale et al. (2005). Planktonic foraminifera biozonation (PFZ) is according to Falzoni and Petrizzo (2020). Calcareous nannofossils biozonation (CNZ) follows Tsikos et al. (2004) and this study. Lithostratigraphy, carbon isotope stratigraphy, oxygen isotope ratio of bulk carbonates and macrofossil shells, and $\Delta^{13}C$ ($\delta^{13}C_{carb} - \delta^{13}C_{org}$) of the Eastbourne section after Gale et al. (2005), Tsikos et al. (2004), Voigt et al. (2006) and Jarvis et al. (2011). Definition of the OAE 2 interval after Jarvis et al. (2011), Gambacorta et al. (2015) and Jenkyns et al. (2017). Identification of the $\delta^{13}C$ positive peaks "a" to "d" follows Jarvis et al. (2006, 2011) and Voigt et al. (2008); $\delta^{13}C_{carb}$ nomenclature after Paul et al. (1999). Plenus Carbon Isotope Excursion (Plenus CIE) according to O'Connor et al. (2020) and Falzoni and Petrizzo (2022) (light blue band). The stratigraphic range of Boreal macrofossils follows Paul et al. (1999) and Gale and Christensen (1996); the latter is based on the Jefferies' collection of Dover deposited in the Sedgwick museum (Cambridge). The stratigraphic range of the dinoflagellate cysts *Cyclonephelium compactum-membraniphorum* is after Pearce et al. (2009) for Eastbourne and Dodsworth (2000) for Lulworth. Planktonic foraminiferal data (*Praeglobotruncana plenusiensis*, *Muricohedbergella kyphoma*) of the Eastbourne section are after Falzoni and Petrizzo (2020, 2022). Stratigraphic intervals characterized by cooling episode(s) during the PCE according to different studies in the references (dark blue bars). For interpretation of the references to colour in this figure legend, the reader is referred to the web version of this article.

the English Chalk (Fig. 2) and elsewhere have been differently interpreted by the authors, O'Connor et al. (2020) suggested to constrain the PCE to the stratigraphic interval between the $\delta^{13}C$ peak "a" and "b" (Plenus CIE in Fig. 2), independently from the evidence for cooling. A similar approach was followed by Falzoni and Petrizzo (2022) who extended the Plenus CIE to below peak "a" to account for the geochemical evidence for cooling from the top of Bed 1 and the occurrence of Boreal species from the base of Bed 2 (Fig. 2). Therefore, the Plenus CIE constrains the stratigraphic interval characterized by one or more episodes of cooling as identified based on the geochemical proxies and/or fossil record. The definition of the PCE by Jenkyns et al. (2017) is followed for the Eastbourne section.

Two distinct events, if present, cannot be stratigraphically resolved in the Vocontian Basin based on the available data (Gale and Christensen, 1996; Gale et al., 2019; Falzoni and Petrizzo, 2022), and the identification of the PCE interval in this section follows Gale et al. (2019).

The influence of cooling during the PCE in the WIS is still subject to debate. No belemnites or other boreal macrofossils entered the WIS in this stratigraphic interval. Evidence of assemblage changes are currently limited to the southward migration of boreal dinoflagellate cysts (Eldrett et al., 2014; van Helmond et al., 2014, 2016) and changes in the dominant coiling direction of *Muricohedbergella delrioensis* coinciding with high $\delta^{18}O$ values (Desmares et al., 2016), which might reflect cooling in analogy with modern species (*Neogloboquadrina pachyderma* vs. *Neogloboquadrina incompta*). However, the duration and effects of the event in the WIS are currently unclear (see Sageman et al., 2024), and for this reason the PCE is not discussed for the Pueblo section.

2.2. Hemipelagic-pelagic sections

2.2.1. Rock Canyon section, Pueblo, Colorado, USA

The Rock Canyon section near Pueblo is situated in the south-central part of the Western Interior Seaway (WIS) (Fig. 1), which was a foreland

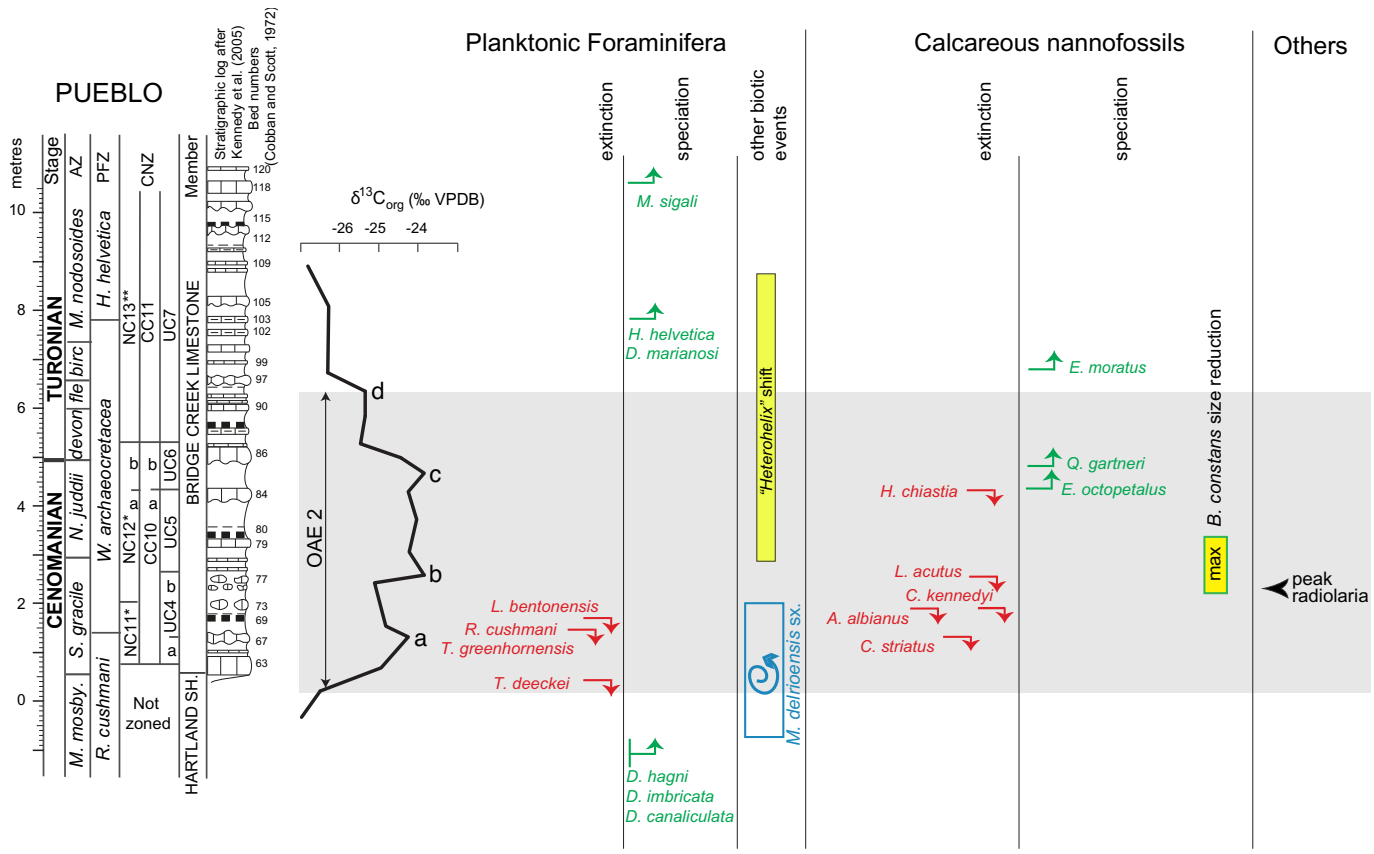

Fig. 3. Rock Canyon section, Pueblo, Colorado (Western Interior Seaway). The Cenomanian/Turonian boundary is placed between the *N. juddii* and the *W. devonense* Zones according to the GSSP definition (Kennedy et al., 2000). Stratigraphic log after Kennedy et al. (2005), bed numbers according to Cobban and Scott (1972). Ammonite biozonation (AZ) is according to Kennedy et al. (1999, 2000). Planktonic foraminifera biozonation (PFZ) follows Caron et al. (2006) and Elderbak and Leckie (2016). Calcareous nannofossils biozonation (CNZ) is according to Watkins (1985), Bralower (1988) and Russo (2014); $\delta^{13}C_{org}$ is according to Pratt and Threlkeld (1984) and Pratt (1985). OAE 2 definition follows Jarvis et al. (2011), Gambacorta et al. (2015) and Jenkyns et al. (2017). Peaks "a" to "d" on the carbon isotope curve are according to Jarvis et al. (2006) and Voigt et al. (2008). Planktonic foraminifera species extinction, speciation, and other biotic events are from Leckie (1985), Eicher and Diner (1985), Leckie et al. (1998), Keller and Pardo (2004), Caron et al. (2006), Desmares et al. (2007, 2016), Elderbak and Leckie (2016) re-interpreted according to Falzoni et al. (2018a). Radiolaria are after Caron et al. (2006). Calcareous nannofossil data are from Bralower (1988), Bralower and Bergen (1998), Watkins (1985) and Russo (2014).
Abbreviations planktonic foraminifera: *L. bentonensis* = *Laeviella bentonensis*; *R. cushmani* = *Rotalipora cushmani*; *T. greenhornensis* = *Thalmanninella greenhornensis*; *T. deeckei* = *Thalmanninella deeckei*; *D. hagni* = *Dicarinella hagni*; *D. imbricata* = *Dicarinella imbricata*; *D. canaliculata* = *Dicarinella canaliculata*; *D. marianosi* = *Dicarinella marianosi*; *H. helvetica* = *Helvetoglobotruncana helvetica*; *M. sigali* = *Marginotruncana sigali*.
Abbreviations calcareous nannofossils: *C. striatus* = *Cretarhabdus striatus*; *A. albianus* = *Axopodorhabdus albianus*; *C. kennedyi* = *Corollithion kennedyi*; *L. acutus* = *Lithraphidites acutus*; *H. chiastia* = *Helenea chiastia*; *E. octopetalus* = *Eprolithus octopetalus*; *Q. gartneri* = *Quadrum gartneri*; *E. moratus* = *Eprolithus moratus*.

basin extending from the Gulf of Mexico, northward to the Arctic Ocean and with a southern prolongation connected to the Atlantic Ocean. The Rock Canyon section is ~12 m-thick and it includes the uppermost Hartland Shale and the lower Bridge Creek Limestone Members of the Greenhorn Formation exposed west of Pueblo (Fig. 3). The Global Stratotype Section and Point (GSSP) for the base of the Turonian Stage is located at the first occurrence of the ammonite *Watinoceras devonense* in Bed 86 (Kennedy et al., 2000, 2005). The Cenomanian/Turonian boundary at Pueblo is one of the best-documented stage boundaries due to the dense fossil record, consisting mainly of ammonites, inoceramids, foraminifera and nannofossils (Kennedy et al., 2000). Ammonite species are well known, owing to the detailed publications of Cobban and Scott (1972), Cobban (1988), Kennedy and Cobban (1991) and Kennedy et al. (1999, 2000). Planktonic foraminifera have been studied by many authors over the last 45 years adopting different sampling resolution and methodologies (i.e., washed residues and thin sections) (Eicher, 1969; Eicher and Worstell, 1970; Eicher and Diner, 1985; Leckie, 1985; Leckie et al., 1998; West et al., 1998; Keller and Pardo, 2004; Keller et al., 2004; Caron et al., 2006; Desmares et al., 2007, 2016; Elderbak et al., 2014; Elderbak and Leckie, 2016; Bryant et al., 2021). In this paper, we use planktonic foraminiferal bioevents derived from all previous studies and reinterpreted according to Falzoni et al. (2018a). Calcareous nannofossils at Pueblo were studied in detail by Watkins (1985), Bralower (1988), Bralower and Bergen (1998), Tsikos et al. (2004), Corbett et al. (2014) and Faucher et al. (2017), and are discussed herein. Morphometric analyses on nannofossils were performed by Faucher et al. (2017).

In this study, we adopt the organic carbon isotope curve by Pratt and Threlkeld (1984) and Pratt (1985), being the most representative, although other carbon isotope records have been generated for the Rock Canyon section and for cores drilled nearby (PU-79 and Portland cores) (Pratt et al., 1993; Keller et al., 2004; Bowman and Bralower, 2005; Caron et al., 2006; Sageman et al., 2006; Desmares et al., 2007).

2.2.2. Gun Gardens section, Eastbourne, UK

The Gun Gardens section at Eastbourne (UK) is situated in the central part of the Anglo-Paris Basin (Fig. 1). The succession is 27 m-thick and consists of alternations of clay-rich (marls) and clay-poor carbonates (calcisphere-, coccolith- and inoceramid-rich limestones called chalks). Boundaries between beds are invariably bioturbated. The succession can

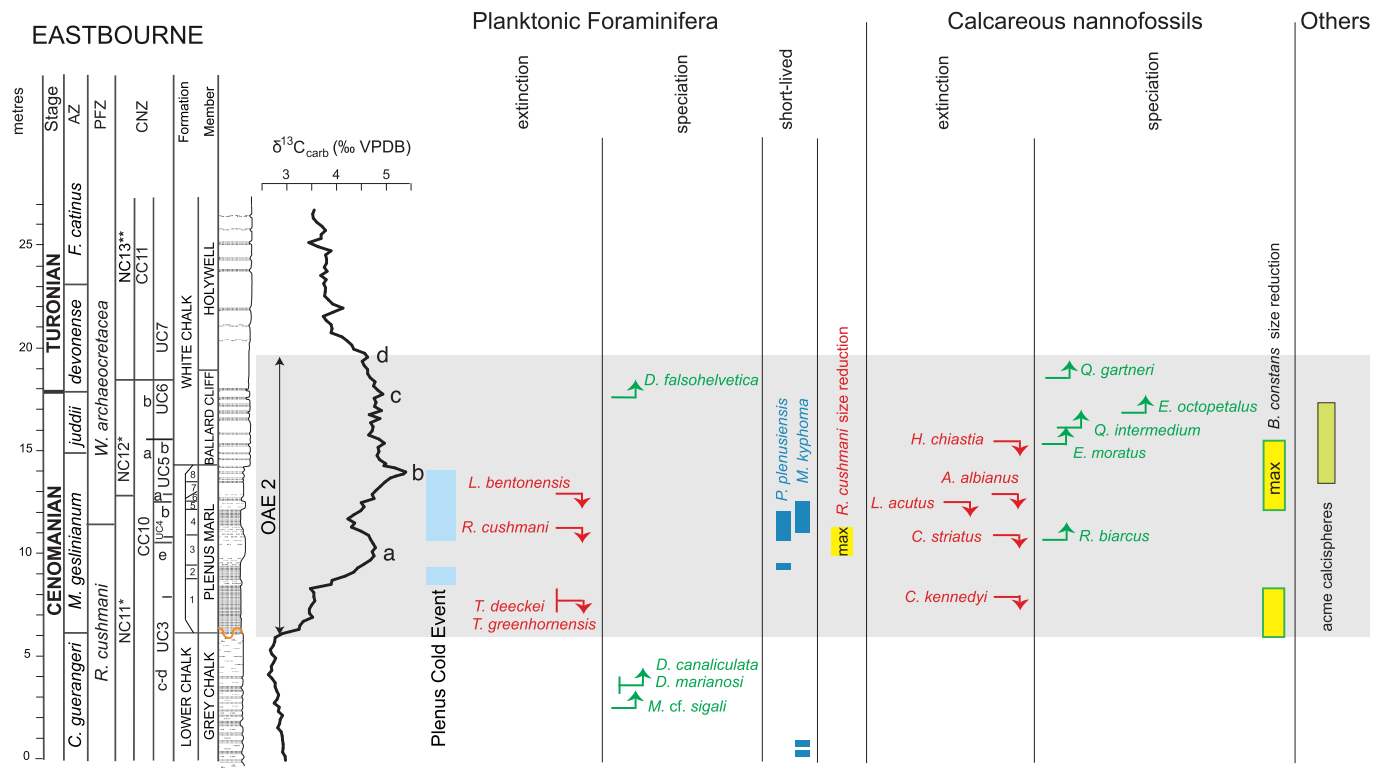

Fig. 4. Gun Gardens section, Eastbourne, SE England (Anglo-Paris Basin). The Cenomanian/Turonian boundary is placed between the *N. juddii* and the *W. devonense* Zones according to the GSSP definition (Kennedy et al., 2000). Ammonite biozonation (AZ) follows Gale et al. (2005). Planktonic foraminifera biozonation (PFZ) is according to Falzoni and Petrizzo (2020). Calcareous nannofossils biozonation (CNZ) follows Tsikos et al. (2004) and this study. Lithostratigraphy after Tsikos et al. (2004); $\delta^{13}C_{carb}$ is according to Tsikos et al. (2004). OAE 2 definition follows Jarvis et al. (2011), Gambacorta et al. (2015) and Jenkyns et al. (2017). Peaks "a" to "d" on the carbon isotope curve are according to Jarvis et al. (2006, 2011) and Voigt et al. (2008). Plenus Cold Event according to Jenkyns et al. (2017). Planktonic foraminifera extinction, speciation, and calcispheres distribution are from Falzoni and Petrizzo (2020, 2022). Size reduction of *R. cushmani* is according to Falzoni et al. (2018b). Calcareous nannofossil data are from Tsikos et al. (2004) and this study.
See caption of Fig. 3 for abbreviations of planktonic foraminifera and calcareous nannofossils and as follows: *D. falsohelvetica* = *Dicarinella falsohelvetica*; *M.* cf. *sigali* = *Marginotruncana* cf. *sigali*; *P. plenusiensis* = *Praeglobotruncana plenusiensis*; *M. kyphoma* = *Muricohedbergella kyphoma*; *Q. intermedium* = *Quadrum intermedium*.

be divided into four distinct units, from the base: the Grey Chalk and the Plenus Marl Members of the Lower Chalk Formation, and the Ballard Cliff and Holywell Members of the White Chalk Formation (Fig. 4) (Gale et al., 2005). This section has been extensively studied in the last 30 years because it is relatively thick and complete, it yields a highly-resolved carbon isotope record from bulk carbonates (Gale et al., 1993; Paul et al., 1999; Tsikos et al., 2004), tolerably well-preserved microfossils (benthic and planktonic foraminifera, nannofossils: Lamolda et al., 1994; Paul et al., 1999; Keller et al., 2001; Hart et al., 2002; Linnert et al., 2011; Faucher et al., 2017; Falzoni and Petrizzo, 2020, 2022) and a diverse macrofauna (ammonites, inoceramids, bivalves: Gale et al., 2000, 2005).

The Plenus Marl Member is a distinctive greenish marly unit pinched in between the two thick carbonate-rich units of the Grey Chalk and White Chalk and crops out at Gun Gardens with the maximum thickness (8 m) found in the Anglo-Paris Basin (Gale et al., 2005). Jefferies (1962, 1963) distinguished 8 beds within the Plenus Marl, based on their lithological features and paleontological content including belemnites (the species *Praeactinocamax plenus*), brachiopods, bivalves, and serpulids with strong boreal affinities. Boreal macrofossils are recognized in Bed 2, 4 to 6, and 8 (Gale and Christensen, 1996; Paul et al., 1999; Jenkyns et al., 2017). However, the Boreal macrofossil fauna is particularly abundant and diverse in Bed 4 suggesting that the maximum cooling occurred during its deposition (Jefferies, 1962; Gale and Christensen, 1996; Paul et al., 1999), a hypothesis supported by oxygen isotopes values obtained on diagenetically screened macrofossils (Voigt et al., 2004, 2006). Following the GSSP definition, the Cenomanian/Turonian boundary is placed at the base of the ammonite *Watinoceras devonense* Zone, which is traced at Eastbourne based on the ammonite and inoceramid assemblage and on the biostratigraphic and carbon isotope correlation with the GSSP section at Rock Canyon (Gale et al., 2005; Kennedy et al., 2005).

We present and discuss species extinctions, speciations and changes in size of planktonic foraminifera using published data (Falzoni et al., 2018a, 2018b; Falzoni and Petrizzo, 2020, 2022), whereas for calcareous nannofossils we integrated published data (Tsikos et al., 2004; Linnert et al., 2011; Faucher et al., 2017) with new high-resolution data acquired for this study.

2.2.3. Clot Chevalier section, Vocontian Basin, SE France

The Clot Chevalier section is located in southeastern France (Fig. 1). The area paleogeographically belongs to the Vocontian Trough, a relatively deep subtropical basin (estimated mid-Cretaceous paleolatitude of ~30°N: Hay et al., 1999; Philip and Floquet, 2000) connected to the Tethyan Ocean. The examined section is 35 m-thick and the sedimentary succession consists of alternating dark grey marlstones and light grey limestones of latest Cenomanian-earliest Turonian age (Gale et al., 2019) (Fig. 5). The section includes a ~ 28 m-thick succession of laminated organic-rich marlstones that belong to the Thomel Level (Crumière, 1990; Morel, 1998) and represent the local equivalent of the Bonarelli Level of the Umbria-Marche Basin (Arthur and Premoli Silva, 1982). Four lithological units within the Thomel Level (Th1-Th4) were defined by Jarvis et al. (2011) in another section of the eastern part of the Vocontian Basin (Pont d'Issole) and recognized at Clot Chevalier. Units Th1 and Th3 consist of grey to dark grey marlstones with modest TOC content (up to 2 wt%) whereas units Th2 and Th4 are primarily

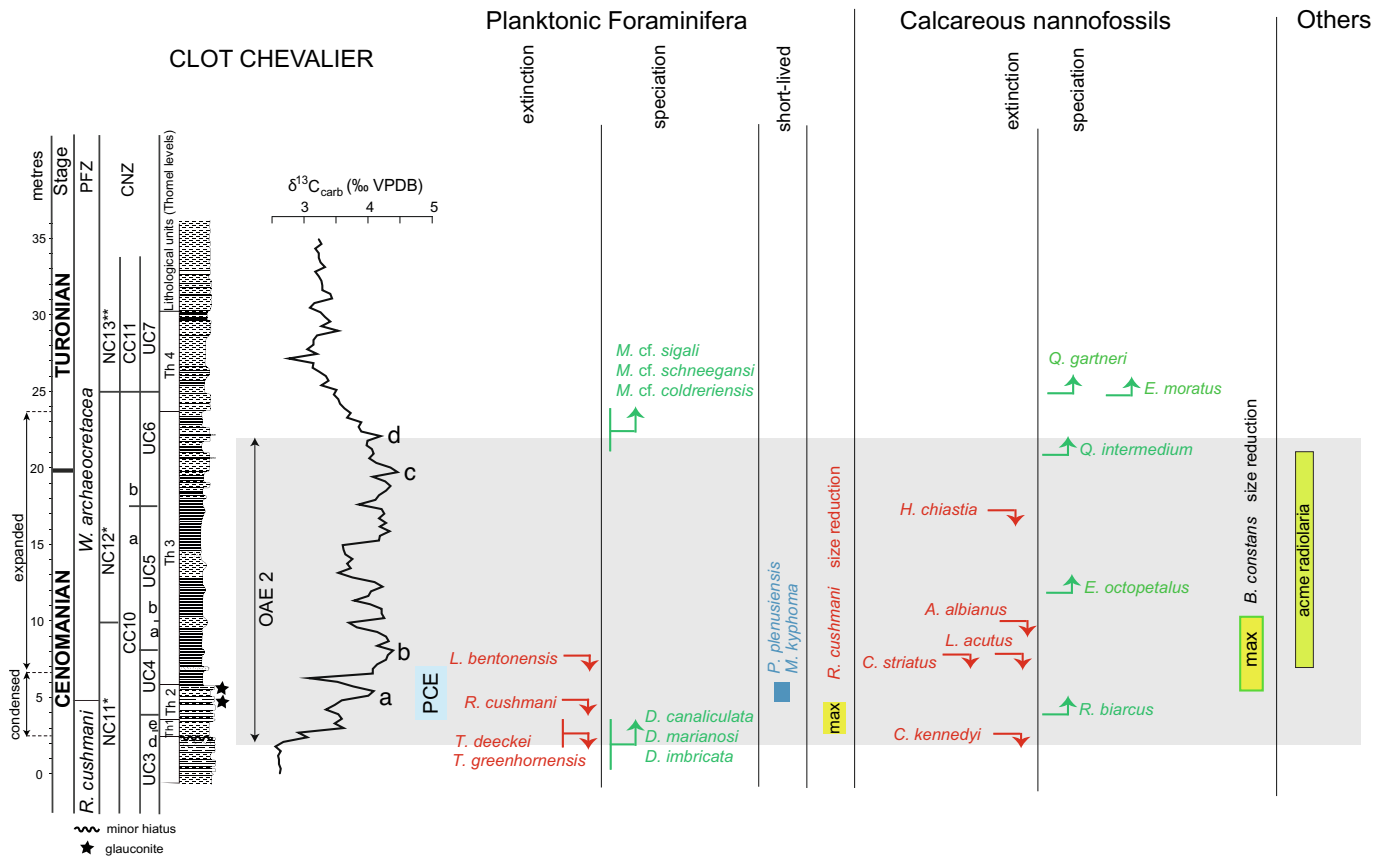

Fig. 5. Clot Chevalier section, SE France (Vocontian Basin). The Cenomanian/Turonian boundary is approximated to peak "c" (Gale et al., 2019). Lithostratigraphy and lithologic units follow Gale et al. (2019). Planktonic foraminifera biozonation (PFZ) follows Falzoni et al. (2016). Calcareous nannofossils biozonation (CNZ), $\delta^{13}C_{carb}$ and Plenus Cold Event (PCE) are according to Gale et al. (2019). Peaks "a" to "d" on the carbon isotope curve are according to Jarvis et al. (2006, 2011) and Voigt et al. (2008). Planktonic foraminifera extinction, speciation, and radiolaria distribution are from Falzoni et al. (2016) and Falzoni and Petrizzo (2020, 2022). Calcareous nannofossil data are from Gale et al. (2019).
See caption of Fig. 3 for abbreviations of planktonic foraminifera and calcareous nannofossils and as follows: *M.* cf. *sigali* = *Marginotruncana* cf. *sigali*; *M.* cf. *schneegansi* = *Marginotruncana* cf. *schneegansi*; *M.* cf. *coldreriensis* = *Marginotruncana* cf. *coldreriensis*; *P. plenusiensis* = *Praeglobotruncana plenusiensis*; *M. kyphoma* = *Muricohedbergella kyphoma*; *Q. intermedium* = *Quadrum intermedium.*

marly limestones (Gale et al., 2019). Sedimentological evidence indicates a hiatus at the base of unit Th1, confirmed by the presence of a burrowed sharp surface. The occurrence of glauconite grains from 4 to 6 m from the base of the section (within units Th1 and Th2) indicates the presence of a condensed stratigraphic interval characterized by a very low sedimentation rate or by brief episodes of interruption of sedimentation. Among microfossils, radiolaria are particularly common in the organic-rich marly layers, planktonic foraminifera and calcareous nannofossils are generally abundant, except in unit Th3 where abundance is low, and the calcareous plankton shows moderate to good preservation (Falzoni et al., 2016; Gale et al., 2019). The section does not yield ammonites or other diagnostic macrofossils, but a Boreal macrofossil assemblage (including *P. plenus*), is documented in a single bed at Les Lattes (Gale and Christensen, 1996; Grosheny et al., 2017) ~20 km to the SE of Clot Chevalier. Lithostratigraphy, biostratigraphy, and carbon isotope correlations suggest that the bed containing Boreal macrofossils at Les Lattes is correlatable with the upper part of unit Th2 at Clot Chevalier (Falzoni and Petrizzo, 2022) and with Bed 4 of the Plenus Marls in the English Chalk (Gale and Christensen, 1996). This interval coincides with a shift toward higher oxygen isotope ratios in bulk carbonates and a pCO_2 drop suggested by a decrease of $\Delta^{13}C$ values (Gale et al., 2019).

The planktonic foraminifera and calcareous nannofossils species extinctions, speciations and changes in size (Falzoni et al., 2016, 2018a, 2018b; Faucher et al., 2017; Gale et al., 2019) are discussed in this study.

2.3. Carbonate platform sections

2.3.1. Raia del Pedale section, Apennine Carbonate Platform, southern Italy

The Raia del Pedale section is located in southern Italy (Fig. 1). It belongs to the Apennine Carbonate Platform (APC), a shallow-water paleogeographic domain, which developed at the southern margin of the Tethyan Ocean from the Late Triassic to the Late Cretaceous (Bernoulli, 2001; Bosellini, 2004). The estimated late Cenomanian paleolatitude of the APC is ~22–24°N (Philip and Floquet, 2000). The section examined for this paper is 70 m-thick (Fig. 6). It consists of meter-scale peritidal cycles deposited in an inner carbonate platform environment (Frijia et al., 2019). Subtidal intervals at the base of the cycles are characterized by LBF, green algae (dasycladaleans and codiaceans), and rudist bivalves (radiolitids). Intertidal and supratidal intervals at the top of the cycles are generally made of microbial laminites. The carbon isotope stratigraphy of the Raia del Pedale section has been previously published by Parente et al. (2008). A detailed sedimentological log can be found in Frijia et al. (2019), along with additional geochemical data (TOC, $\delta^{13}C_{org}$ and $\delta^{15}N_{bulk}$). The record of other geochemical proxies has been produced for the OAE 2 interval of the Raia del Pedale section ($\delta^{7}Li$, Pogge von Strandmann et al., 2013; $\delta^{238}U_{carb}$, Clarkson et al., 2018). The extinctions and speciations of LBF are from Parente et al. (2008).

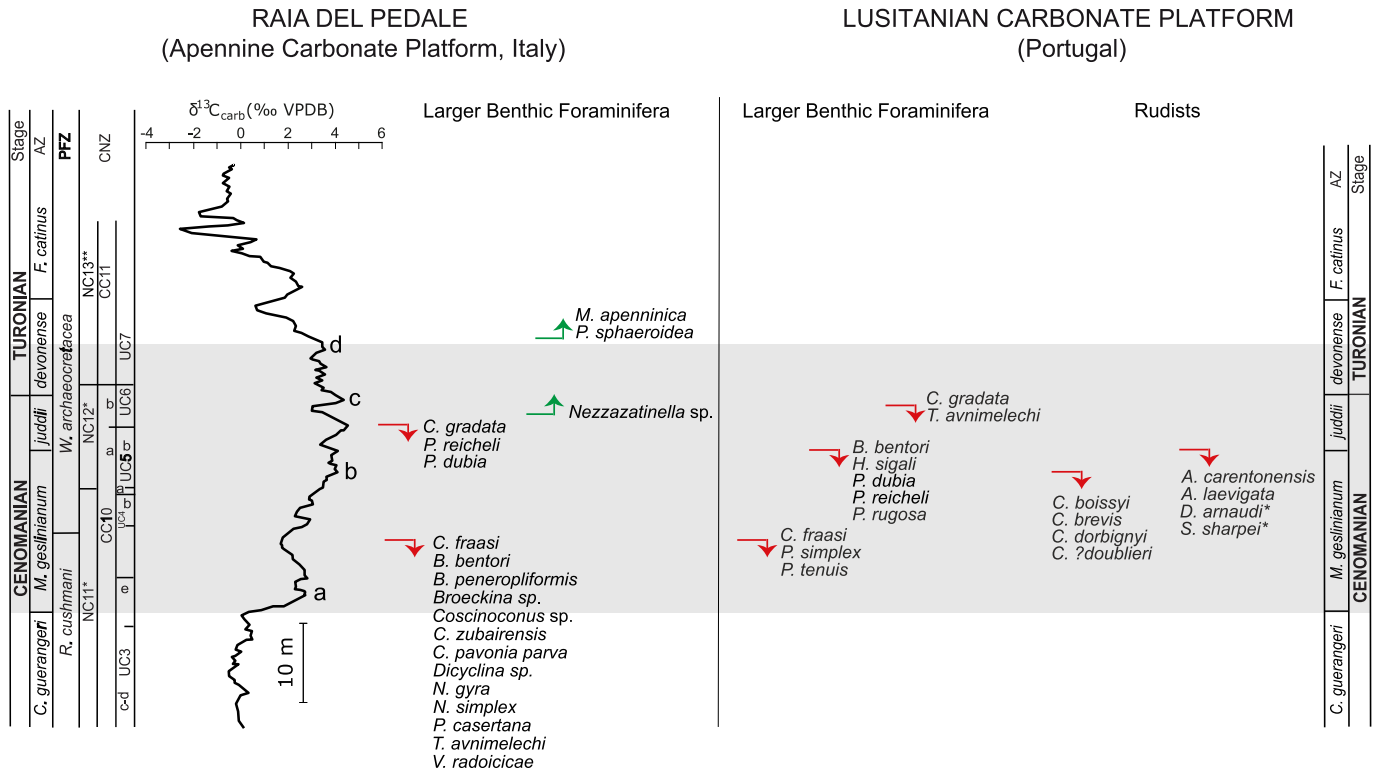

Fig. 6. Larger Benthic Foraminifera and rudists bioevents in the Raia del Pedale section (Apennine Carbonate Platform, southern Italy) and in the Lusitanian Carbonate Platform (Portugal). Raia del Pedale section: $\delta^{13}C_{carb}$ and the Larger Benthic Foraminifera (LBF) extinction events are from Parente et al. (2008); the speciations events are from Arriaga et al. (2016); the chronostratigraphic calibration of the section is derived from correlation by carbon isotope stratigraphy with the reference section of Eastbourne. Lusitanian Carbonate Platform: data on LBF and rudists are from Berthou (1984); chronostratigraphic calibration of the bioevents is based on ammonite biostratigraphy (see Fig. 8 in Berthou, 1984).
Abbreviations LBF: *B. bentori* = *Biconcava bentori; B. peneropliformis* = *Biplanata peneropliformis; C. fraasi* = *Cisalveolina fraasi; C. gradata* = *Chrysalidina gradata; C. zubairensis* = *Coxites zubairensis; C. pavonia parva* = *Cuneolina pavonia parva; H. sigali* = *Hemicyclammina sigali; M. apenninica* = *Moncharmonti apenninica; N. gyra* = *Nezzazata gyra; N. simplex* = *Nezzazata simplex; P. simplex* = *Praealveolina simplex; P. tenuis* = *Praealveolina tenuis; P. rugosa* = *Pseudocyclammina rugosa; P. sphaeroidea* = *Pseudocyclammina sphaeroidea; P. reicheli* = *Pseudolituonella reicheli; P. dubia* = *Pseudorhapydionina dubia; P. casertana* = *Pseudorhipidionina casertana; T. avnimelechi* = *Trochospira avnimelechi; V. radoicicae* = *Vidalina radoicicae.*
Abbreviations rudists: A. carentonensis = *Apricardia carentonensis; A. laevigata* = *Apricardia laevigata; C. boissyi* = *Caprinula boissyi; C. brevis* = *Caprinula brevis; C. dorbignyi* = *Caprinula dorbignyi; C.? doublieri* = *Caprinula? doublieri; D. arnaudi* = *Durania arnaudi; S. sharpei* = *Sauvagesia sharpei*. The two species of radiolitid (calcite-dominated) rudists marked with an asterisk are known from Turonian levels in carbonate platforms of other localities (see explanation in the text).

2.3.2. *Dataset for rudist bivalves*

Data for rudist bivalves (Hippuritida Newell, 1965) used in this study are from a compilation of ranges of genera (Steuber et al., 2016), reviewed and evaluated in the context of the evolution of benthic carbonate producers and carbonate platforms (Mitchell, 2023; Steuber et al., 2023). These compilations are at the substage level, and detailed systematic studies of the stratigraphical distribution of rudist taxa in upper Cenomanian sections that have a reliable carbon isotope stratigraphy are still missing. For most regions, either a precise biostratigraphical framework for upper Cenomanian rudist-bearing deposits is absent (e.g., Bauer et al., 2004), or detailed taxonomic data for rudists are lacking in sections that have a well-established chemostratigraphy (e.g., Křížová et al., 2024). Detailed biostratigraphic correlations at the level of ammonite zones have been established for the upper Cenomanian of the Lusitanian Platform at the eastern margin of the Atlantic Ocean (Berthou, 1984) and of the Provence Platform at the northwestern Tethyan margin (Philip and Airaud-Crumiere, 1991) and were extrapolated to the carbonate platforms of north African and Levantine Tethyan margin (Philip et al., 2024).

3. Results

3.1. *Hemipelagic-pelagic sections*

3.1.1. *Rock Canyon section, Pueblo, Colorado, USA*

3.1.1.1. Planktonic foraminifera. Extinctions of planktonic foraminiferal species are observed in the lower part of OAE 2 (below peak "b"), in stratigraphic order from the bottom to the top (Fig. 3): *Thalmanninella deeckei* in the interval between the onset of OAE 2 and peak "a" (Keller and Pardo, 2004); *Thalmanninella greenhornensis*, *Rotalipora cushmani* and the planispiral species *Laeviella bentonensis* between peaks "a" and "b" (Eicher and Diner, 1985; Leckie, 1985; Keller and Pardo, 2004; Caron et al., 2006; Desmares et al., 2007). Atypical specimens that resemble *R. cushmani*, but with smaller size, fewer chambers and a thin keel, have been reported by Desmares et al. (2007) and Leckie (1985) below bed 86 in between peak "b" and "c". However, we do not include these specimens in *R. cushmani* because of their morphological differences and ecologically controlled stratigraphic record. Speciations are documented outside the OAE 2 interval (Fig. 3) with the lowest occurrence (LO) of *Dicarinella* species (*D. hagni*, *D. imbricata*, *D. canaliculata*) below the onset of OAE 2 (Caron et al., 2006) and of *Helvetoglobotruncana helvetica*, *Dicarinella marianosi* and *Marginotruncana sigali* above the event (Caron et al., 2006; Elderbak and Leckie, 2016).

Additional events include a sharp increase (up to the 45 %) in the abundance of sinistral *M. delrioensis* (Desmares et al., 2016) from below the onset of OAE 2 to the trough between peaks "a" and "b", followed by the onset of the *Heterohelix* shift (a sharp increase of the abundance of biserial taxa up to the 50 % of the assemblage, after Leckie, 1985 and Leckie et al., 1998) slightly above peak "b" (Leckie et al., 1998). Caron et al. (2006) also reported a peak in the abundance of radiolaria slightly preceding the *Heterohelix* shift.

3.1.1.2. Calcareous nannofossils. Extinctions and speciations of calcareous nannoplankton species are encountered throughout OAE 2 in the following stratigraphic order (Fig. 3): the HO (highest occurrence) of *Cretarhabdus striatus* is right above peak "a" (Russo, 2014); the HOs of *Corollithion kennedyi* and *Axopodorhabdus albianus* are reported in correspondence of the trough between peaks "a" and "b" (Bralower, 1988); the HO of *Lithraphidites acutus* is associated to peak "b" (Watkins, 1985; Bralower and Bergen, 1998); the LO of *Eprolithus octopetalus* (Russo, 2014) and the HO of *Helenea chiastia* (Bralower, 1988) are in correspondence of peak "c"; the LO of *Quadrum gartneri* is just prior to peak "d" (Watkins, 1985) and the LO of *Eprolithus moratus* is above peak "d" (Russo, 2014). *Quadrum intermedium* and *Rotelapillus biarcus* were not identified (Watkins, 1985; Bralower, 1988; Russo, 2014).

3.1.2. Gun Gardens section, Eastbourne, UK

3.1.2.1. Planktonic foraminifera. Extinctions are identified in the lower part of OAE 2 (below peak "b"), in stratigraphic order from the bottom to the top (Fig. 4): the HO of *T. deeckei* and *T. greenhornensis* in the same sample in the middle part of the first $\delta^{13}C$ build-up (below peak "a"), the extinction of *R. cushmani* in the trough between peaks "a" and "b", and of *L. bentonensis* about 1 m below peak "b". Most speciations are documented below the onset of OAE 2 and include the LO of *Marginotruncana* cf. *sigali* and of *Dicarinella* species (*D. canaliculata* and *D. marianosi*) (Falzoni and Petrizzo, 2020). The LO of *Dicarinella falsohelvetica* occurs in correspondence of peak "c" (Fig. 4).

Other events include the occurrence of short-lived species (i.e., *Praeglobotruncana plenusiensis* and *Muricohedbergella kyphoma*) ranging from 50 cm below peak "a" to below peak "b", except for two samples at the base of the section yielding very rare *M. kyphoma* specimens (Falzoni and Petrizzo, 2022). The acme in the abundance of calcispheres occurs from 50 cm below peak "b" to peak "c" (Falzoni and Petrizzo, 2020) (Fig. 4). The *Heterohelix* shift and the LO of *H. helvetica* reported by Keller et al. (2001) in this section were not confirmed by subsequent studies in thin section and washed residue samples (Tsikos et al., 2004; Falzoni et al., 2018a).

3.1.2.2. Calcareous nannofossils. Extinctions and speciations of calcareous nannoplankton species are encountered throughout OAE 2 following this stratigraphic order (Fig. 4): the HO of *C. kennedyi* is in the lower part of the first $\delta^{13}C$ build-up, i.e. ca 2 m below peak "a" (Tsikos et al., 2004; this study). The LO of *R. biarcus* and the HO of *C. striatus* are just above peak "a" at the beginning of the $\delta^{13}C$ trough (this study). The HO of *L. acutus* (this study) and the HO of *A. albianus* (Tsikos et al., 2004) just precede peak "b". The LO of *E. moratus* (this study), the HO of *H. chiastia* and the LO of *Q. intermedium* correspond to the middle part of the $\delta^{13}C$ plateau (this study). The LO of *E. octopetalus* occurs just below peak "c" (this study) and the LO of *Q. gartneri* is just above peak "c" (Tsikos et al., 2004).

3.1.3. Clot Chevalier section, Vocontian Basin, SE France

3.1.3.1. Planktonic foraminifera. Extinctions are identified in the lower part of OAE 2 (below peak "b"), in stratigraphic order from the bottom to the top (Fig. 5): *T. deeckei* and *T. greenhornensis* in the lower part of the first $\delta^{13}C$ build-up below peak "a", followed by the extinction of *R. cushmani* close to peak "a" and by the extinction of *L. bentonensis* close to peak "b". Speciations include the LO of some *Dicarinella* species (*D. marianosi*, *D. imbricata*, *D. canaliculata*) below peak "a" and of *Marginotruncana* species (*M.* cf. *coldreriensis*, *M.* cf. *schneegansi*, *M.* cf. *sigali*) slightly above peak "d".

Other events are represented by the occurrence of short-lived species (*P. plenusiensis* and *M. kyphoma*) from below peak "a" to the trough between peak "a" and peak "b", followed by the acme of radiolaria from below peak "b" to below peak "d" (Falzoni and Petrizzo, 2022).

3.1.3.2. Calcareous nannofossils. Extinctions and speciations are encountered throughout OAE 2 in the following stratigraphic order (Gale et al., 2019): the HO of *C. kennedyi* is at the onset of the $\delta^{13}C$ positive excursion; the LO of *R. biarcus* is in correspondence of peak "a"; the HO of *L. acutus* and the LO of *C. striatus* are close to peak "b"; the HO of *A. albianus* and the LO of *E. octopetalus* are just after peak "b"; the HO of *H. chiastia* is in correspondence of peak "c"; the LO of *Q. intermedium* is at peak "d"; and the LO of *Q. gartneri* and the LO of *E. moratus* are just above peak "d" (Fig. 5).

3.2. Carbonate platform sections

3.2.1. LBF at Raia del Pedale, Apennine Carbonate Platform, southern Italy

High-diversity LBF assemblages are present in the lower part of the section, up to the relative minimum in $\delta^{13}C$ values occurring between the positive peaks "a" and "b" (Fig. 6). Within this interval, 16 species of LBF have been identified: *Biconcava bentori*, *Biplanata peneropliformis*, *Broeckina* sp., *Chrysalidina gradata*, *Cisalveolina fraasi*, *Coscinoconus* sp., *Coxites zubairensis*, *Cuneolina pavonia parva*, *Dicyclina* sp., *Nezzazata gyra*, *N. simplex*, *Pseudolituonella reicheli*, *Pseudorhapydionina dubia*, *Pseudorhipidiniona casertana*, *Trochospira avnimelechi*, *Vidalina radoicicae*. The range of *C. fraasi* is actually very short, as this species occurs only in a 5 m-thick interval in the lower part of OAE 2 (Fig. 6). The disappearance of *C. fraasi* coincides with the HO of most of the species listed above. This is the first step of LBF extinction described in Parente et al. (2008). The only three species of LBF occurring above this level are *C. gradata*, *P. reicheli* and *P. dubia*. These three "survivors" disappear about 15 m above, within the plateau of the $\delta^{13}C$ excursion (Fig. 6). This represents the second step of LBF extinction described in Parente et al. (2008). Above this level, the benthic foraminiferal assemblages consist of *Nezzazatinella* sp., whose LO is just above the second step of LBF extinction, associated with small and simple morphotypes of miliolids and textulariids (see also Arriaga et al., 2016). New species appear above the OAE 2 interval, starting with *Pseudocyclammina sphaeroidea* and *Moncharmontia apenninica* (Fig. 6).

3.2.2. Rudists bivalves and Larger Benthic Foraminifera in the Lusitanian Carbonate Platform

The Cenomanian-Turonian boundary interval marks a very significant extinction among rudist bivalves, with a reduction in the number of genera of more than 50 % (Steuber et al., 2023). It is remarkable that this reduction is predominantly caused by the loss of genera with aragonite-dominated shells, while calcite-dominated taxa were not affected and then expanded significantly in the middle and upper Turonian (Philip and Airaud-Crumiere, 1991; Steuber et al., 2023). Following the Cenomanian extinction, new aragonite-dominated rudist genera only occurred in the mid-Campanian (Steuber et al., 2016). While these patterns are obvious at the substage level, a higher stratigraphical resolution and detailed records of extinctions are scarce, because of the typically low resolution of the biostratigraphy of shallow-water benthos.

Relatively high-resolution biostratigraphic data are available from the Lusitanian Carbonate Platform (Fig. 6), at the eastern margin of the Atlantic Ocean (Berthou, 1984; Callapez, 2003), from the Provence Platform, at the northern margin of Tethys (Philip and Airaud-Crumiere, 1991), and from the carbonate platforms at the north African and north

Arabian margins of southern Tethys (Philip et al., 2024). The extinction of aragonite-dominated taxa (caprinulids and caprinids, *Ichthyosarcolites*) is reported within the *Metoicoceras geslinianum* ammonite Zone (Berthou, 1984) or at the boundary between the *M. geslinianum* and *Neocardioceras juddii* Zones (Philip and Airaud-Crumiere, 1991; Philip et al., 2024). The latest Cenomanian rudist associations, after the extinction of aragonite-dominated taxa, consist mainly of radiolitids. Three steps of extinctions are recorded for LBF in the Lusitanian Platform (Berthou, 1984). Alveolinids (*Praealveolina simplex, P. tenuis* and *C. fraasi*) disappear in the middle part of the *geslinianum* ammonite Zone; *P. reicheli*, *P. dubia*, *Pseudocyclammina rugosa* and *Hemicyclammina sigali* disappear at the top of the *M. geslinianum* Zone; the HO of *C. gradata* and *T. anvimelechi* is in the upper part of the *N. juddii* Zone (Fig. 6).

In many regions, carbonate platform growth continues up to the Cenomanian/Turonian boundary where it is typically interrupted by a hiatus and condensed sedimentation including most of the lower Turonian.

4. Discussion

4.1. The response of biocalcifiers to OAE 2 from basin to platform

4.1.1. Planktonic foraminifera

Planktonic foraminifera experienced four extinctions and four to six speciations in the studied sections across the latest Cenomanian-earliest Turonian. All extinctions fall within the OAE 2 interval, between the onset of OAE 2 and peak "b", and follow the same sequence in the three studied sections (Fig. 7): first the highest occurrences (HO) of *Thalmanninella* species (*T. deeckei* and *T. greenhornensis*) below peak "a" in the lower part of the first build-up, followed by the HO of *R. cushmani* within the trough between peaks "a" and "b", and finally the HO of *L. bentonensis* just below peak "b". The extinctions of these species are broadly synchronous among the studied sections, and generally across mid-low latitudes (Falzoni et al., 2018a). The only exceptions are represented by the delayed extinction (above peak "a") of *T. greenhornensis* at Pueblo (Fig. 7), possibly reflecting persisting favourable ecologic conditions for this species in the WIS, and by the earlier extinction of rotaliporids at Clot Chevalier (Fig. 7), which might be biased by the presence of a condensed stratigraphic interval around peak "a" (Falzoni et al., 2016; Gale et al., 2019). In the Eastbourne and Clot Chevalier sections, morphometric analysis performed on *R. cushmani* show fluctuations of the test size within a 150 μm range and a maximum size reduction of ~200 μm prior to its extinction (Falzoni et al., 2018b). The occurrence and maximum abundances (see also Falzoni and Petrizzo, 2022) of the short-lived species (*P. plenusiensis* and *M. kyphoma*) correspond to the PCE interval at Eastbourne and Clot Chevalier (Fig. 7).

Speciations are only observed immediately before the onset of OAE 2 and after the termination of the event, except for the LO of *D. falsohelvetica* that is identified only at Eastbourne among the studied sections, and in correspondence of peak "c" (Fig. 7). All the new evolving species belong to the double keeled genera *Dicarinella* and *Marginotruncana*, except for the single-keeled *Helvetoglobotruncana helvetica.* The evolutionary first appearance of the genus *Dicarinella* is recorded in the middle Cenomanian within the Mid Cenomanian Event 1 (Petrizzo and Gale, 2023) and is followed by the appearance of *Marginotruncana* species slightly below the onset of OAE 2 at Eastbourne (Fig. 7) and after the termination of OAE 2 at Clot Chevalier and Pueblo (Fig. 7). *Dicarinella* and especially *Marginotruncana* diversify significantly after OAE 2 and are commonly found in tropical-subtropical assemblages from the Turonian to the Santonian. *Helvetoglobotruncana helvetica* is only recognized with certainty at Pueblo (Fig. 7) because its identification at Eastbourne (Keller et al., 2001) was not confirmed by subsequent studies (Tsikos et al., 2004; Falzoni et al., 2018a). Moreover, its first occurrence is diachronous across mid-low latitudes (e.g., Caron et al., 2006; Huber and Petrizzo, 2014, and references therein) and is likely controlled by local paleoenvironmental conditions.

Other events among planktonic foraminifera include the *Heterohelix* shift from peak "b" to above "d" (Fig. 7), although the top of the event may be diachronous among sections (Leckie et al., 1998; West et al., 1998). The *Heterohelix* shift is documented throughout the WIS (Leckie, 1985; Leckie et al., 1998; West et al., 1998; Keller et al., 2004; Elderbak et al., 2014; Bryant et al., 2021), the central Atlantic (Tsikos et al., 2004; Falzoni et al., 2018a), and in the Tethyan domain (Nederbragt and Fiorentino, 1999; Caron et al., 2006; Bomou et al., 2013; Kalanat and Vaziri-Moghaddam, 2019; Ouikene et al., 2022).

4.1.2. Calcareous nannofossils

Across the OAE 2 interval, calcareous nannofossils experienced five extinctions and four speciations. These bioevents characterize the whole OAE 2 and its aftermath (Fig. 7). Four out of five extinctions (*C. kennedyi*, *C. striatus*, *A. albianus*, *L. acutus*) occur between the onset of OAE 2 and peak "b", whereas the extinction of *H. chiastia* is registered shortly before peak "c". Speciations start above peak "b", except for the appearance of *R. biarcus,* which is recorded between the onset of OAE 2 and peak "a". The LO of *Q. intermedium* at Eastbourne is between peaks "b" and "c", at Clot Chevalier is above peak "c" whereas it is absent at Pueblo. The LO of *E. octopetalus* is in the interval between peaks "b" and "c". The LO of *E. moratus* at Eastbourne is between peaks "b" and "c" whereas at Pueblo and Clot Chevalier is above peak "d". The LO of *Q. gartneri* is, instead, commonly identified just above peak "c" or slightly above peak "d".

Nannofossil biostratigraphic data, available for sections in different basins and settings, show the reproducibility and synchroneity of the HO of *C. kennedyi, A. albianus, L. acutus* and *H. chiastia* as well as the LO of *Q. gartneri* (e.g., Bralower, 1988; Tsikos et al., 2004; Hardas and Mutterlose, 2006; Linnert et al., 2010, 2011; Gale et al., 2019; this study). Remarkably, the species going extinct are all represented by coccoliths (except for *L. acutus*) whereas speciations are of nannoliths or nococcoliths. Moreover, most taxa going extinct (with the only exception of *H. chiastia*) are characterized by short stratigraphic range as they appeared in the middle Albian or early Cenomanian.

Morphometric investigations revealed coeval size variations of *B. constans* coccoliths, which are affected by average-size reduction in the lowermost part of OAE 2 with smallest specimens occurring around peak "b" (Faucher et al., 2017) (Fig. 7).

4.1.3. Large Benthic Foraminifera (LBF)

At Raia del Pedale, LBF show two steps of extinctions within the OAE 2 interval (Fig. 7). The first one occurred at the relative minimum in $\delta^{13}C$ values between the positive peaks "a" and "b" and severely reduced the number of species (from 16 to 3 species). The second step occurred above peak "b", within the plateau of $\delta^{13}C$ excursion, eliminated the three survivors and left a benthic foraminiferal fauna consisting only of very simple and small forms, with no LBF. Some originations occurred within the OAE 2 interval (*Nezzazatinella* sp.), just after the second step of LBF extinction or immediately above it (*M. apenninica* and *P. sphaeroidea*). However, it is worth noticing that these newcomers are very small and simple species that would not qualify as LBF neither in terms of size nor in terms of architectural complexity. The two-steps pattern of extinction of LBF documented at Raia del Pedale is also recorded in other sections of the Apennine Carbonate Platform (Parente et al., 2008) and the same pattern has been reported from other Tethyan carbonate platforms (Fleury, 1971; Chiocchini et al., 1994; Solak et al., 2020).

In the Lusitanian Platform of Portugal a similar pattern of extinction is recorded, with the alveolinids disappearing in the middle part of the *M. geslinianum* Zone and other five species of LBF disappearing at the top of the *M. geslinianum* Zone, with only two species having their HO in the uppermost part of the *N. juddii* Zone (Fig. 7; based on data in Berthou, 1984). As to the consistency of this pattern on a global scale, it must be taken into account that in many carbonate platform sections the exact stratigraphic position of the HO of LBF species, with reference to the

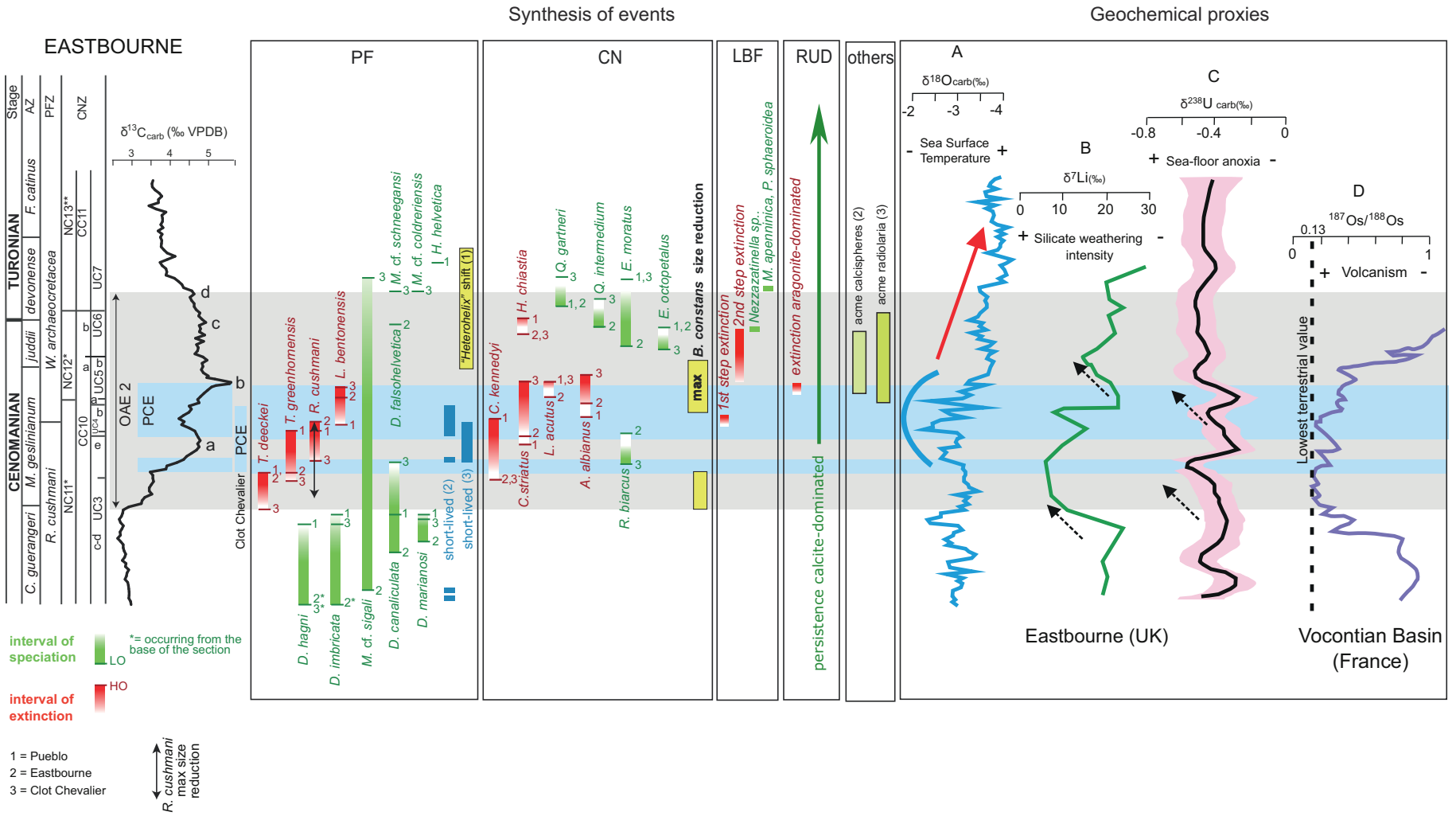

Fig. 7. Comparison of the timing of the bioevents of calcareous plankton and shallow-water benthic calcifiers and correlation with the record of geochemical proxies. The carbon isotope stratigraphy of Eastbourne is used to tie the correlation from basin to platform and to tie bioevents and geochemical proxies. Definition of OAE 2 and PCE, and the nomenclature of the carbon isotope excursion as in Figs. 2 and 4. The PCE interval as defined at Clot Chevalier in Fig. 5 is shown.

Geochemical proxies: A) $\delta^{18}O_{carb}$, as a proxy of sea surface temperature, from Tsikos et al. (2004); B) $\delta^{7}Li$, as a proxy of the silicate weathering intensity, from Pogge von Strandmann et al. (2013); C) $\delta^{238}U_{carb}$, as a proxy of the extent of sea-floor anoxia, from Clarkson et al. (2018); D) $^{187}Os/^{188}Os$, as a proxy of LIP volcanism, from Du Vivier et al. (2014). Abbreviations: PF = Planktonic Foraminifera; CN = Calcareous Nannofossils; LBF = Larger Benthic Foraminifera; RUD = Rudist Bivalves.

OAE 2 interval, is unknown or incorrectly placed, due to the lack of ammonite or carbon isotope calibration (Simmons and Bidgood, 2023). Despite the limitation imposed by poor chronostratigraphic calibration, compilations of the stratigraphic ranges of LBF at the species (Neumann and Schroeder, 1985) and genus level (Steuber et al., 2023) show a very significant extinction at or close to the Cenomanian/Turonian boundary and are therefore compatible with the high-resolution record of the Apennine Carbonate Platform and of the Lusitanian Carbonate Platform, which show that extinctions occurred within the OAE 2 interval. On the other hand, the list of survivors, whose stratigraphic range extends beyond OAE 2 in the lower Turonian, is continuously growing (e.g. Schlagintweit and Yazdi-Moghadam, 2021). These survivors either imply the existence of refugia, where conditions favourable to LBF persisted during OAE 2, or call for the existence of biological traits granting resilience to OAE 2 paleoenvironmental perturbations. The existence of refugia is clearly witnessed by the Western Platform of Peru, where an endemic fauna of LBF thrived during the OAE 2 interval (Consorti et al., 2018 and references therein).

4.1.4. Rudists

The significant extinction event in the evolution of rudist bivalves in the Cenomanian-Turonian boundary interval is well established (Philip and Airaud-Crumiere, 1991; Steuber et al., 2016, 2023), but a precise stratigraphy of the demise of individual taxa is only available for limited regions and remains to be established on a global scale. Several carbon isotope records of carbonate platforms across OAE 2 are available and some of them have been used to establish late Cenomanian extinction patterns, e.g., among LBF (Parente et al., 2008; Frijia et al., 2015), but none of the latest Cenomanian rudist records can be confidently linked to carbon isotope stratigraphy, with the exception of some papers, which document fluctuations in the abundance of rudist remains but without data on the taxonomic composition of rudist associations (e.g., Křížová et al., 2024). In the sections from the Lusitanian platform, ammonite biostratigraphy can be used to define the rudist bioevents at a resolution comparable with that achieved by carbon isotope stratigraphy. The currently available data highlight that the late Cenomanian rudist extinction event occurred within the OAE 2 interval (Fig. 7). In particular, the demise of aragonite-dominated genera occurred below the top of the *M. geslinianum* Zone (Berthou, 1984), while the proliferation of carbonate platforms with calcite-dominated shells (radiolitids) continued into the latest Cenomanian.

While the high sea-level during the late Cenomanian favoured the widespread development of rudist-bearing carbonate platforms along the northern and southern margins of Tethys (Philip, 1998; Steuber and Löser, 2000), the development of Cenomanian carbonate platforms in the Americas was very limited, and only a few low-diversity rudist associations are known from southern and central-east Mexico (Mitchell, 2023). No rudist records are available for the lowermost Turonian of the Americas, and cosmopolitan hippuritids only occur in the uppermost and middle Turonian. Very few isolated occurrences are reported from the WIS. Therefore, patterns of turnover related to the Cenomanian-Turonian boundary event in the Americas are largely unknown (Mitchell, 2023).

4.2. A synthesis of bioevents across OAE 2 from pelagic basins to carbonate platforms

A comparison of bioevents from pelagic-hemipelagic settings to carbonate platforms highlights the following patterns across OAE 2 (Fig. 7):

(1) There was no extinction at the onset of OAE 2, neither in planktonic nor in shallow-water benthic biocalcifiers, apart from the local HO of *T. deeckei* at Clot Chevalier.
(2) The planktonic foraminifera, *T. deeckei,* disappeared in the first build-up phase of the CIE, below peak "a" at both Pueblo and Eastbourne. During this first phase of OAE 2 both LBF and rudists were highly diverse and were not affected by extinctions.
(3) The interval between peaks "a" and "b" shows the largest number of biotic events among both planktonic and shallow-water benthic calcifiers (Fig. 7). Among planktonic foraminifera, there was the extinction of *R. cushmani* (preceded by a decrease in size), *T. greenhornensis* and *L. bentonensis* and the occurrence of two short-lived species (*P. plenusiensis* and *M. kyphoma*). Three species of calcareous nannofossils have their HO in this interval (*A. albianus*, *C. striatus, L. acutus*). Moreover, *B. constans* shows a distinct decrease in coccolith size, with minimum size reached at peak "b". The first step of extinction of LBF also occurred within this interval. It affected the alveolinids and most of the other species, which became extinct, leaving only three survivors. The extinction of aragonite-dominated rudists can also be placed at the top of this interval, as it has been correlated with a level below the top of the *M. geslinianum* Zone, which can be equated with peak "b" of the CIE.
(4) The interval between peaks "b" and "c" records some extinctions and several speciations. The LBF species that survived the first step of extinction were eliminated within this interval (second step of extinction, Fig. 7). For planktonic foraminifera, the so-called *Heterohelix* shift is recorded in the WIS and in many other sections from the central Atlantic to the Tethyan domain across this interval and extends above the termination of the OAE 2 interval. The HO of the calcareous nannofossil *H. chiastia* is also recorded between peaks "b" and "c" along with the LO of three species (*Q. intermedium*, *E. octopetalus, E. moratus*) albeit with some diachrony among the three studied sections (Fig. 7). The LO of *Q. gartneri* is recorded within the interval between peak "c" and "d". Among LBF, one new species appears above peak "b" (*Nezzazatinella* sp.) and two species just above peak "d" (*M. apenninica* and *P. sphaeroidea*). These species are included in LBF by most authors, even if they would not qualify as LBF, for their small size and simple architecture. Some species of radiolitid rudists (*D. arnaudi* and *S. sharpei*) are reported to have their HO within the upper part of the OAE 2 interval in the Lusitanian Carbonate Platform (Fig. 6) (Berthou, 1984; Philip et al., 2024). However, it is worth mentioning that the taxonomic status of some of these species is uncertain (Steuber, 1999; Salama and Özer, 2019) and that they have been reported also from younger Turonian levels in other localities (De Castro and Sirna, 1996; Özer and Ahmad, 2016; http://www.paleotax.de/rudists/).

4.3. Linking the OAE 2 biotic events to proxies of paleoenvironmental perturbations

OAE 2 is a global perturbation of the carbon cycle, witnessed by the positive CIE and accompanied by a series of extreme paleoenvironmental changes that potentially acted as stressors and drove a significant biotic response. It is listed as a mass extinction that eliminated approximately 26 % of marine genera (Sepkoski, 1996; Harries and Little, 1999; Bambach, 2006). We analyzed the record of some fossil groups that were among the dominant carbonate producers in pelagic-hemipelagic settings and carbonate platforms: planktonic foraminifera, calcareous nannofossils, LBF and rudists. In this subchapter, we will look at the time-relations between the biotic events and the record of geochemical proxies of paleoenvironmental perturbations, and will discuss potential causal links.

In Fig. 7, we plotted the oxygen isotope ratio ($\delta^{18}O_{carb}$) as a proxy of sea surface temperature (SST) (Tsikos et al., 2004), the lithium isotope ratio ($\delta^{7}Li$) as a proxy of the silicate weathering intensity (Pogge von Strandmann et al., 2013), the uranium isotope ratio ($\delta^{238}U_{carb}$) as a proxy of the extent of sea-floor anoxia (Clarkson et al., 2018), and the osmium isotope ratio ($^{187}Os/^{188}Os$) as a proxy of submarine volcanism (Du Vivier et al., 2014). The carbon isotope curve ($\delta^{13}C_{carb}$) of the

Eastbourne section (Tsikos et al., 2004) is used as the standard time-framework for the geochemical proxies and the bioevents. Fig. 7 highlights clearly that during the first phase of OAE 2, the increase of volcanic activity (which actually started before the onset of the event), silicate weathering intensity, and extent of seafloor anoxia did not impact significantly the main biocalcifiers. The only bioevents in this interval are the diachronous disappearance of *T. deeckei* and the first episode of size-reduction of *B. constans* coccoliths, the latter possibly responding to volcanogenic CO_2 emissions (Faucher et al., 2017).

As discussed previously, for both planktonic and shallow benthic biocalcifiers the most significant bioevents are recorded in the interval between peak "a" and "b". This interval coincides with the significant SST fluctuations documented during the PCE at Eastbourne and in many other basins (Fig. 7). Among planktonic foraminifera, extinctions involved the last representatives of the genera *Thalmanninella* and *Rotalipora* (Fig. 7) that have been traditionally interpreted as thermocline dwellers and require a thermally stratified water column in oligotrophic regimes (e.g., Caron and Homewood, 1983; Leckie, 1987; Hart, 1999; Huber et al., 1999; Petrizzo et al., 2008a). Therefore, their extinction indicates a perturbation that affected the thermocline, such as the disruption of the water column stratification, and/or a shift from a strictly oligotrophic to a more mesotrophic regime. The extinction of *R. cushmani* coinciding with the acme of cooling during the PCE in the Anglo-Paris and Vocontian Basins (Figs. 3, 4), the occurrence of short-lived planktonic foraminiferal species with stratigraphic ranges paralleling those of the Boreal macrofossils at Eastbourne, the coeval geochemical variations suggesting changes in ocean circulation patterns (Zheng et al., 2013; O'Connor et al., 2020), and the re-oxygenation of bottom waters (Jenkyns et al., 2017; Clarkson et al., 2018), are all indicative of a disruption of ocean stratification during the PCE. This disruption might be explained by the southward inflow of cool and more mesotrophic surface waters in the Anglo-Paris and Vocontian Basins (Falzoni and Petrizzo, 2022).

Laeviella bentonensis likely inhabited the cool/winter mixed layer in oligo-mesotrophic regimes and in a relatively well-stratified water column (e.g., Caron and Homewood, 1983; Leckie, 1987; Huber et al., 1999; Petrizzo et al., 2008a; Elderbak and Leckie, 2016; Falzoni and Petrizzo, 2020). The extinction of this species indicates a perturbation that might have affected the mixed layer possibly associated with an increase in sea-surface nutrients, which is consistent with a pulse of increased intensity of silicate weathering, based on the δ^7Li record (Fig. 7).

The extinctions of calcareous nannoplankton species do not represent an extinction event, as they are distributed over at least 100 ky (Sageman et al., 2006) in all studied sections. Three out of four species go extinct in the interval between peak "a" and "b" (*A. albianus*, *C. striatus*, *L. acutus*). *Corollithion kennedyi* goes extinct just prior to peak "a" and *H. chiastia* disappears close to peak "c". As far as the PCE is concerned, it appears that four nannoplankton extinctions occur within the PCE (Fig. 7).

The coccolith size reductions of individual nannofossil species, such as *B. constans*, do not temporally coincide with the extinctions. In fact, an initial decrease in average coccolith size is observed prior to peak "a", with the climax reached around peak "b". Regarding *B. constans* coccolith size, temperature and nutrient availability in surface waters do not seem to have been decisive factors. Instead, ocean chemistry, related to CO_2 concentration and carbonate saturation state, has been considered central in coccolith production by *B. constans*, leading to recurrent reductions in size (Faucher et al., 2017). In general, the first phase of OAE 2, up to peak "b", was characterized by massive emissions of volcanic CO_2 during the formation of the Caribbean Plateau (Neal et al., 2008; Percival et al., 2024), which likely induced a decrease of carbonate saturation that was detrimental to some calcareous nannoplankton species, temporarily resulting in the production of dwarf *B. constans* coccoliths. Additionally, the biocalcification processes may have also been affected by bio-limiting metals from hydrothermal plumes that fertilized the global ocean and pumped toxic metals into the system (Faucher et al., 2017; Bryant et al., 2021).

The disruption of ocean stratification and the delivery of nutrient-rich waters to isolated low-latitude shallow-water platforms was proposed as the main cause of mass extinction of LBF during OAE 2 (Parente et al., 2008). This hypothesis was based on two arguments. LBF as a group can be considered as K-strategists (i.e., organisms characterized by long life cycle and low reproductive potential) adapted to nutrient-poor conditions (Hottinger, 1982; Hallock, 1985, 2000). Extinction during OAE 2 affected first the larger and more complex LBF (i.e. alveolinids), which are supposedly the most extreme oligotrophs, and later the smaller and less complex taxa. This two-steps pattern was interpreted as due to the passing of two thresholds of nutrification during OAE 2 (Parente et al., 2008), paralleling the ecological succession along a gradient of increasing nutrient input observed in field studies of nutrient-polluted habitats of LBF (Hallock, 2000). Even if the hypothesis of extinction driven by increased nutrient levels is appealing for LBF, it does not explain why rudists were also affected and especially why aragonite-dominated rudists were the main victims. In fact, rudists were epifaunal suspension feeders, seemingly adapted to mesotrophic environments. The hypothesis that rudists hosted symbionts (Kauffman and Johnson, 1988), has not passed the scrutiny of subsequent studies, except for very few, rare taxa (Gili and Götz, 2018, and references therein). Therefore, rudists are not expected to be negatively impacted by the increase of nutrient levels driven by a collapse of the thermal stratification of the ocean. On the other hand, the selective extinction of aragonite-dominated rudists and the greater resilience of calcite-dominated ones is consistent with a decrease of seawater carbonate saturation (Steuber et al., 2023). This could be linked to the collapse of thermal stratification and to the invasion of the shallow-water tropics with cool and CO_2-rich water masses during the PCE.

Planktonic foraminifera do not show extinctions or speciations between peaks "b" and "c", except for the appearance of *D. falsohelvetica*, which is very rare and only documented in the Anglo-Paris Basin (Desmares et al., 2020) and Algeria (Ouikene et al., 2022). However, they register a significant change in the composition of the assemblage between peaks "b" and "c", represented by the acme of biserial taxa (*Heterohelix* shift). The *Heterohelix* shift has been traditionally related to periods of unstable environmental conditions characterized by a poorly stratified water column and increased nutrient concentrations in surface waters (Leckie, 1985; Leckie et al., 1998; West et al., 1998). In stratigraphic sections where the *Heterohelix* shift is not documented (e.g., Eastbourne and Clot Chevalier), radiolaria and calcispheres dominate the microfossils assemblages and suggest a widespread shift to a meso-eutrophic regime. The increased concentration of nutrients could have been triggered, at least in coastal waters, by another episode of increased silicate weathering intensity recorded by the δ^7Li proxy above peak "b" (Fig. 7). The second step of extinction of LBF also occurred between peaks "b" and "c". It could be related to the passing of a further threshold in nutrient concentration, which affected the few LBF species that survived the first step of extinction (Parente et al., 2008).

Four new species of calcareous nannofossils show their LOs in an interval going from half-way between peaks "b" and "c" to just above peak "d". However, these bioevents are diachronous, and some of them were probably influenced by local factors (e.g., *E. moratus*, *E. octopetalus*). The time interval corresponding to the appearance of new species of calcareous nannofossils is associated with a partial size recovery of *B. constans*, likely linked to a decrease in trace metals and CO_2, in relation to reduced volcanic activity (Faucher et al., 2017, and $^{187}Os/^{188}Os$ proxy in Fig. 7). It is interesting to note that these species are all nannoliths, which are more heavily calcified compared to coccoliths. One might speculate that these forms are related to a recovery of the alkalinity following the interval of reduced carbonate saturation highlighted by the size reduction of *B. constans* coccoliths.

Speciations of planktonic foraminifera prior and after OAE 2 (Fig. 7) mainly occur within the double keeled genera *Dicarinella* and

Marginotruncana, which are interpreted as intermediate to thermocline dwellers that lived in oligo-mesotrophic regimes, although some species belonging to the genus *Dicarinella* also thrived in a more weakly stratified upper water column (Petrizzo et al., 2020; Falzoni and Petrizzo, 2022). Therefore, speciations among double-keeled taxa prior to OAE 2 might have been favoured by the differentiation of ecological niches within a thermally stratified upper water column, where rotaliporids probably represented the deepest and most oligotrophic dwellers. After OAE 2, the diversification of double-keeled taxa may have been also triggered by the availability of new ecological niches at the thermocline depth, which were previously occupied by rotaliporids.

Figure 7 shows that planktonic foraminifera and calcareous nannoplankton experienced different evolutionary patterns. In fact, although both groups were affected by similar numbers of extinctions and speciations, the timing of the positive and negative phases were very different. The speciation phase (five LOs) of planktonic foraminifera predates the onset of OAE 2 when nannofossil assemblages remain constant. The extinction phase is the same for planktonic foraminifera and calcareous nannofossils: it correlates with the core of the chemostratigraphic anomaly and appears associated with the PCE. The latest part of OAE 2 testifies rather constant planktonic foraminiferal assemblages but is characterized by an origination phase of calcareous nannoplankton. These patterns suggest that calcareous phyto- and zooplankton reacted differently during the OAE 2 precursor and recovery intervals, perhaps because autotrophs (phyto-plankton) and heterotrophs (zoo-plankton) have a different rate of evolutionary response when new niches become available.

4.4. Significance of extinction and resilience of calcareous plankton and benthos across OAE 2

In the previous subchapters we used the record of some key sections to resolve the details of the response of the main biocalcifiers of pelagic-hemipelagic settings and carbonate platforms to the paleoenvironmental perturbations associated with OAE 2. The main merit of this approach is that it allows a high-resolution comparison of the timing of the bioevents from basins to platforms and of the timing of bioevents with the main fluctuations of geochemical proxies. However, by concentrating on a limited number of sections covering only the narrow stratigraphic interval of OAE 2, we could not address a fundamental question: how significant was the impact of OAE 2 on the long-term evolutionary history of the main biocalcifiers?

In Fig. 8 we show a compilation of the number of genera and species of planktonic foraminifera and calcareous nannofossils and of the number of genera of rudists and larger benthic foraminifera across the Albian-Santonian interval. The dataset of Fig. 8 supports the well-known fact that OAE 2 did not represent a major turnover in the evolutionary history of planktonic foraminifera and calcareous nannofossils (see for instance Leckie et al., 2002; Erba, 2004; Steuber et al., 2023). For planktonic foraminifera there were some extinctions within genera during the late Cenomanian, but a much larger number of genera survived and extinctions were compensated by new originations, so that the Turonian records an increase in the number of species. For calcareous nannofossils the long-term number of genera shows a moderate increase with three new genera appearing across the Cenomanian-Turonian boundary interval. Conversely, the number of species shows a two-step decrease in the same interval although the short-term curve

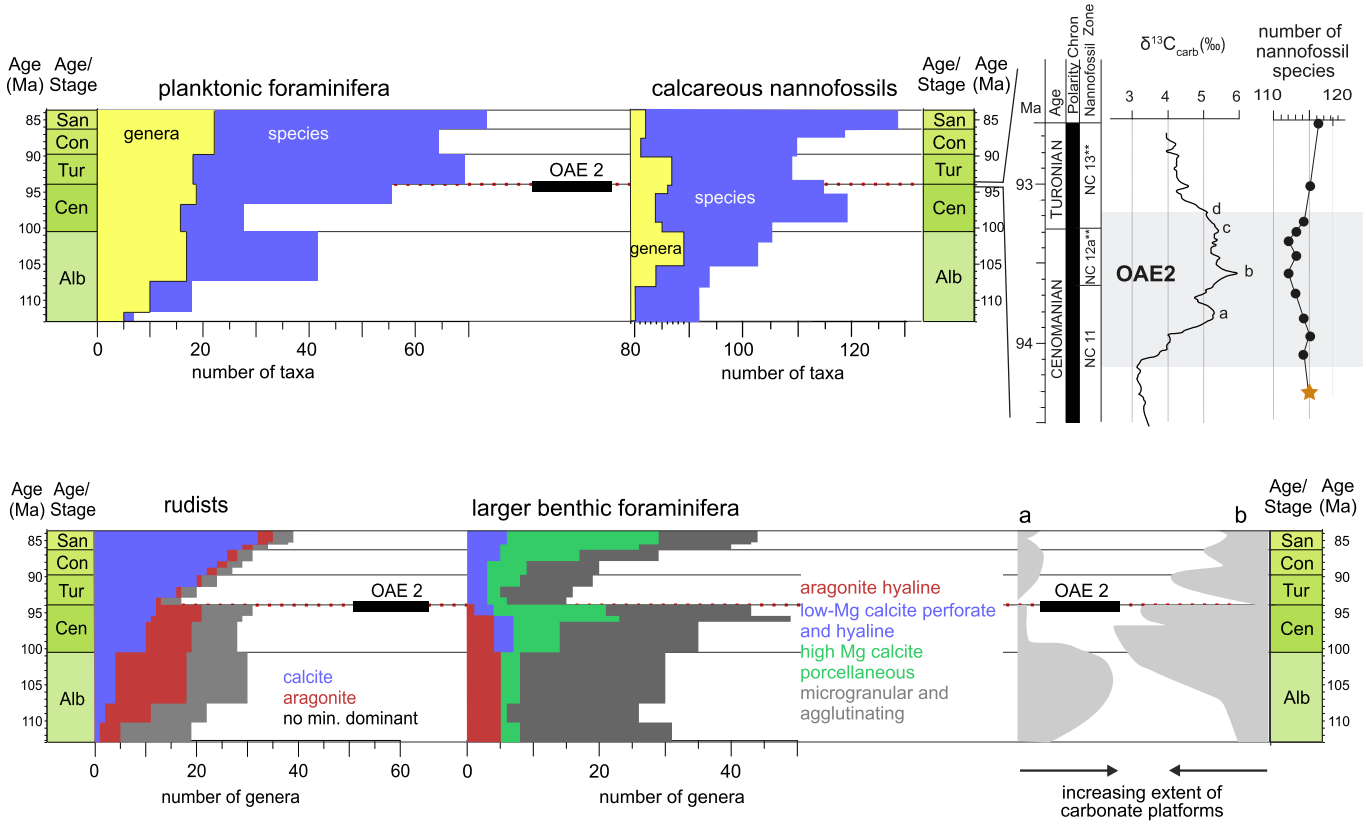

Fig. 8. Compilation of the number of genera and species of planktonic foraminifera and calcareous nannofossils, and of the number of genera of rudists and Larger Benthic Foraminifera (LBF) during the Albian-Santonian time interval. Data for planktonic foraminifera are after the pforams@mikrotax portal (Huber et al., 2016). Data for calcareous nannofossils are from Bown et al. (2004) and this study (OAE 2 detail). Data for LBF and rudists are from Steuber et al. (2023). Extent of carbonate platforms in the Americas (a) and Europe, north Africa and the Middle East (b) from Skelton (2003). The compilation shows that OAE 2 was a mass extinction for LBF and rudists while it did not represent a significant turnover event for planktonic foraminifera and calcareous nannoplankton.

indicates that extinctions and originations are interfingered, thus the total number of nannofossil species after OAE 2 is the same as before the onset of the event.

On the contrary, the OAE 2 and the Cenomanian-Turonian boundary intervals represent a very important extinction event for LBF and rudists (Fig. 8; Philip and Airaud-Crumiere, 1991; Parente et al., 2008; Steuber et al., 2016). Actually, only the end-Cretaceous mass extinction scored higher than the Cenomanian-Turonian boundary event in terms of reduction of diversity (Steuber et al., 2023). The main question that arises from the data of Fig. 8 is: why carbonate platform biocalcifiers were much more vulnerable than planktonic biocalcifiers?

The late Cenomanian-early Turonian interval represents the thermal maximum for the Cretaceous, with open-ocean surface temperatures (SST) estimates at tropical latitudes of >35 °C (Forster et al., 2007; O'Brien et al., 2017). Significantly higher SST could have been reached in the shallow water masses on top of carbonate platforms, as suggested by recent data on the Upper Cretaceous carbonates of the Adriatic Carbonate Platform (Křížová et al., 2024).

Rapid climate change and extreme fluctuations of seawater temperature have been postulated to cause marine extinctions (Reddin et al., 2020 and reference therein), with proposed thresholds for the major Phanerozoic mass-extinctions of magnitudes >5.2 °C and rates >10 °C/Myr (Song et al., 2021). Even faster rates of changes could have been at work during past episodes of rapid climate change, as it has been demonstrated that maximum rates are systematically underestimated in the geological record (Kemp et al., 2015).

The detrimental effect of high temperatures has been demonstrated for several modern species of LBF (Hallock et al., 1993; Schmidt et al., 2011, 2014; Doo et al., 2014; Fujita et al., 2014; Prazeres et al., 2017; Kawahata et al., 2019; Kinoshita et al., 2021). Arguments supporting the vulnerability of rudists to thermal stress can be gained by looking at some large bivalves such as *Pinna* and *Crassostrea*, which have been shown to be endangered by extremely high SST (Fleury et al., 2020; Hernandis et al., 2023).

If climate warming and rapid fluctuations of SST were the main cause of extinction during the OAE 2 interval, there are several possible explanations of why LBF and rudists were much more affected than planktonic foraminifera and calcareous nannofossils. Tropical benthic taxa tend to be more vulnerable to extinction, probably because of their smaller and more fragmented geographic range (Finnegan et al., 2015), especially during hyperthermals (Reddin et al., 2019). Moreover, aragonitic and photosymbiotic taxa tend to have higher extinction risks at hyperthermals (Reddin et al., 2020), which would be another factor explaining the pattern of extinction during OAE 2, when photosymbiotic LBF and aragonite-dominated rudists paid the highest toll. Other ecological factors that could explain the greater vulnerability to extinction of LBF and rudists compared to planktonic foraminifera and calcareous nannofossils are their larger body size and stenothermic ecology (McKinney, 1997).

Ocean acidification has been proposed as a cause of some mass extinction events, especially for those that featured tropical hypercalcifiers among the main victims (Kiessling and Simpson, 2010; Hönisch et al., 2012). OAEs are prime candidates for ocean acidification, because they are caused by the increase of the atmospheric pCO_2 forced by Large Igneous Provinces (LIP) volcanic activity (Greene et al., 2012; Hönisch et al., 2012; Jones et al., 2023). It is worth recalling that the massive injection of volcanogenic CO_2 in the atmosphere-ocean system will result in ocean acidification only if it happens on time scales of less than c. 50 kyr, as for longer time scales the dynamics of the lysocline would act as a buffer and maintain carbonate saturation (Zeebe, 2001; Hönisch et al., 2012).

For OAE 2, ocean acidification has been proposed based on Ca isotopes (Du Vivier et al., 2015; Kitch et al., 2022), on the occurrence of carbonate-poor lithologies (Erba, 2004; Petrizzo et al., 2022; Jones et al., 2023), and on the dwarfism of the calcareous nannofossil *B. constans* (Faucher et al., 2017). However, for OAE 2 there is no compelling geochemical evidence from boron isotopes of a significant decrease in ocean pH, like that produced for other mass extinction events (e.g., Clarkson et al., 2015 and Jurikova et al., 2020 for the end-Permian; Trudgill et al., 2021 for the end-Triassic; Müller et al., 2020 for the early Toarcian; Henehan et al., 2019 for the end-Cretaceous).

Comparison of the biotic response of LBF, rudists, planktonic foraminifera and calcareous nannofossils across the OAE 2 interval can be used to assess the role played by ocean acidification. LBF were heavily affected, but aragonitic taxa, which should have been more vulnerable to ocean acidification, disappeared mainly before OAE 2, after a long-term decline starting in the Early Cretaceous (Steuber et al., 2023). Among rudists, the selective extinction of aragonite-dominated taxa and the greater resilience of calcite-dominated ones is consistent with ocean acidification (Steuber et al., 2023) but could also be the result of the higher vulnerability of aragonitic taxa during hyperthermals (Reddin et al., 2020).

Across OAE 2, planktonic foraminifera assemblages do not show evidence of ocean acidification as documented for other warming events in the geological record (e.g., the increased fragmentation and dissolution of shells during Paleocene-Eocene Thermal Maximum, Petrizzo et al., 2008b) and in modern assemblages (e.g., lighter shells, increased shell porosity: Moy et al., 2009; Iwasaki et al., 2019). The size reduction documented for *R. cushmani* prior to its extinction (Fig. 7) does not seem related to a decrease of ocean $CaCO_3$ saturation, as the last representatives of this species are typically heavily calcified with thick and raised spiral sutures and ridges on the umbilical side. On the other hand, extinctions among planktonic foraminifera involve species that thrived in thermally stratified oligotrophic waters and are concentrated in the PCE interval (Fig. 7), thus are more probably related to the disruption of the sea-surface stratification likely associated to an increased supply of nutrients.

For calcareous nannofossils, the global occurrence of size reduction of *B. constans* coccoliths across the OAE 2 interval has been interpreted as a response to ocean acidification (Faucher et al., 2017), as documented also for OAE 1a (Erba et al., 2010). However, the calcareous nannofossil signal of ocean acidification is much more subdued for OAE 2 compared to the Valanginian Weissert event, which recorded a significant decline of calcite paleofluxes, and to the early Aptian OAE 1a, for which a calcification crisis has been documented at global scale (Erba and Tremolada, 2004; Erba et al., 2010; Erba and Parente, 2024).

In conclusion, the pattern of vulnerability and resilience of LBF, rudists, planktonic foraminifera and calcareous nannofossils across the OAE 2 interval support the hypothesis that ocean acidification was not the main stressor but probably played a role in conjunction with rapid increase and fluctuations of SST, which ultimately caused changes in the ocean circulation patterns and thermal stratification.

5. Conclusions

OAE 2 was a global perturbation of the carbon cycle, accompanied by a series of extreme paleoenvironmental changes that drove a significant biotic response: approximately 26 % of marine genera were extinct during the event. In this study we analyzed the record of the main groups of Cretaceous marine biocalcifiers: planktonic foraminifera, calcareous nannoplankton, large benthic foraminifera (LBF) and rudist bivalves. We used high-resolution data from well-dated sections to compare the timing of biotic events from pelagic-hemipelagic settings to low-latitude carbonate platforms using carbon isotope stratigraphy to establish a common time-framework. We used the same approach to tie the record of biotic events to the record of geochemical proxies of paleoenvironmental changes, looking for potential causes of extinction. Finally, we looked at the wider picture offered by compilations of stratigraphic ranges of species and genera to assess the significance of OAE 2 on the long-term evolutionary history of the main biocalcifiers. The main conclusions that can be drawn from our study are:

1. The first phase of OAE 2, from the onset of the CIE to peak "a", records the extinction of only two species in the studied groups of marine biocalcifiers (*T. deeckei* and *C. kennedyi*). Geochemical proxies indicate that significant paleoenvironmental stressors were already at work during this interval. LIP volcanic activity started before the onset of OAE 2, as recorded by the $^{187}Os/^{188}Os$ record. The massive injection of volcanogenic CO_2 into the ocean-atmosphere system caused global warming and rising SST (recorded by the $\delta^{18}O$ proxy) and stimulated higher intensity of continental weathering (witnessed by the $\delta^{7}Li$ proxy), which both concurred to increasing the extent of seafloor anoxia (recorded by the $\delta^{238}U_{carb}$ proxy). However, our data suggest that these paleoenvironmental stressors did not pass the threshold of resilience neither for planktonic nor for shallow-water benthic biocalcifiers.
2. The interval between peaks "a" and "b" shows the largest number of biotic events among both planktonic and shallow-water benthic calcifiers. Three species of planktonic foraminifera (*R. cushmani, T. greenhornensis* and *L. bentonensis)* and three species of calcareous nannofossils (*A. albianus*, *C. striatus* and *L. acutus*) have their HO in this interval. Moreover, the coccoliths of *B. constans* show a distinct decrease in size. The first step of extinction of LBF also occurred within this interval, eliminating the alveolinids (which are the largest and most complex LBF) and most of the other species. The extinction of aragonite-dominated rudists can be placed at peak "b". The interval between peaks "a" and "b", corresponding to part of the PCE, was characterized by extreme fluctuations of SST, with cooling episodes alternating with peaks of very high temperature. Disruption of ocean stratification during the PCE seems to be a key factor driving the first step of extinction of LBF and of the single keeled and more specialized planktonic foraminifera. The first step of extinction of LBF within the PCE may be also related to overfeeding stress and increased competition for space in high nutrients surface water during the cooling episodes. The increase of the SST at the end of the PCE seems to be the most probable cause of extinction of the aragonite-dominate rudists and of the second step of extinction of the LBF with the concurrent contribution of decreased seawater carbonate saturation.
3. Compilations of the stratigraphic ranges of species and genera of the studied groups of biocalcifiers confirm that planktonic foraminifera and calcareous nannoplankton were much more resilient than LBF and rudists across the OAE 2 interval. The event actually did not represent a major turnover for calcareous plankton while it was a mass extinction for LBF and rudists. There are at least three potential explanations for the higher vulnerability of LBF and rudists under a scenario of extremely high and fluctuating SST as the main cause of extinction: tropical benthic taxa tend to be more vulnerable to extinction during hyperthermals; larger organisms have been shown to be more vulnerable to extinction during hyperthermals; much higher temperatures were probably reached by the shallow water masses on top of carbonate platforms compared to the open ocean. Moreover, LBF hosted photosymbionts, which is another trait that has been shown to enhance vulnerability during hyperthermals, and aragonite-dominated rudists were much more heavily affected than calcite-dominated rudists, which is also expected during hyperthermals.

CRediT authorship contribution statement

Maria Rose Petrizzo: Writing – review & editing, Writing – original draft, Methodology, Data curation, Conceptualization. **Mariano Parente:** Writing – review & editing, Writing – original draft, Data curation, Conceptualization. **Francesca Falzoni:** Writing – review & editing, Writing – original draft, Data curation, Conceptualization. **Cinzia Bottini:** Writing – review & editing, Writing – original draft, Data curation, Conceptualization. **Gianluca Frijia:** Writing – review & editing, Writing – original draft. **Thomas Steuber:** Writing – review & editing, Writing – original draft, Conceptualization. **Elisabetta Erba:** Writing – review & editing, Writing – original draft, Data curation, Conceptualization.

Declaration of competing interest

The authors declare that they have no known competing financial interests or personal relationships that could have appeared to influence the work reported in this paper.

Acknowledgments

The authors are indebted to R. Mark Leckie and an anonymous reviewer for their thoughtful suggestions that greatly improved the final version of the manuscript. Editorial work of the Editor and the Guest Editors of the Special Issue *Biocalcifier resilience and response during global climate changes* is gratefully acknowledged. Andy S. Gale is thanked for providing the geographic coordinates of the Clot Chevalier section. Funding was provided by the Italian Ministry of University and Research (MUR) projects PRIN 2017RX9XXY to EE, PRIN 2022WEZR44 to CB, and by University of Ferrara Fir 2021 to GF.

Appendix A. Taxonomic list

Taxonomic list of species and genera, with author(s) and year of description mentioned in the text and figures, listed in alphabetical order for each fossil group.

Ammonite
Metoicoceras geslinianum (D'Orbigny, 1841)
Neocardioceras juddii (Barrois and Guerne, 1898)
Watinoceras devonense Wright and Kennedy, 1981
Belemnite
Praeactinocamax plenus (Blainville, 1827)
Benthic Foraminifera
Biconcava bentori Hamaoui and Saint-Marc, 1970
Biplanata peneropliformis Hamaoui and Saint-Marc, 1970
Genus *Broeckina* Munier-Chalmas, 1882
Chrysalidina gradata d'Orbigny, 1939
Cisalveolina fraasi (Gümbel, 1872)
Genus *Coscinoconus* (Leupold in Leupold and Bigler, 1936)
Coxites zubairensis Smout, 1956
Cuneolina pavonia parva Henson, 1948
Genus *Dicyclina* Munier-Chalmas, 1887
Hemicyclammina sigali Maync, 1953
Moncharmontia apenninica (De Castro, 1966)
Genus *Nezzazatinella* Darmoian, 1976
Nezzazata gyra (Smout, 1956)
Nezzazata simplex Omara, 1956
Praealveolina simplex Reichel, 1936
Praealveolina tenuis Reichel, 1933
Pseudocyclammina rugosa (d'Orbigny, 1850)
Pseudocyclammina sphaeroidea Gendrot, 1968
Pseudolituonella reicheli Marie, 1954
Pseudorhapydionina dubia (De Castro, 1965)
Pseudorhipidiniona casertana (De Castro, 1965)
*Trochospira avnimelech*i Hamaoui and Saint-Marc, 1970
Vidalina radoicicae Cherchi and Schroeder, 1986
Bivalves
Apricardia carentonensis (d'Orbigny, 1850)
Apricardia laevigata (d'Orbigny, 1842)
Caprinula boissyi (d'Orbigny, 1840)
Caprinula brevis Sharpe, 1850
Caprina dorbignyi Sharpe, 1850
Caprinula? *doublieri* (d'Orbigny, 1850)
Crassostrea Sacco, 1897
Durania arnaudi (Choffat, 1891)

Oxytoma seminudum (Dames, 1874)
Pinna Linnaeus, 1758
Sauvagesia sharpei (Bayle, 1857)
Calcareous nannofossils
Genus *Axopodorhabdus* Wind and Wise in Wise and Wind, 1977
Axopodorhabdus albianus (Black, 1967) Wind and Wise in Wise and Wind, 1977
Genus *Biscutum* Black in Black and Barnes, 1959
Biscutum constans (Górka, 1957) Black in Black and Barnes, 1959
Genus *Corollithion* Stradner, 1962
Corollithion kennedyi Crux, 1981
Genus *Cretarhabdus* Bramlette and Martini, 1964
Cretarhabdus striatus (Stradner, 1963) Black, 1973
Genus *Eprolithus* Stover, 1966
Eprolithus moratus (Stover), Burnett 1998
Eprolithus octopetalus Varol, 1992
Genus *Helenea* Worsley, 1971
Helenea chiastia Worsley, 1971
Genus *Lithraphidites* Deflandre, 1963
Lithraphidites acutus Verbeek and Manivit in Manivit et al., 1977
Genus *Quadrum* Prins and Perch-Nielsen in Manivit et al., 1977
Quadrum gartneri Prins and Perch-Nielsen in Manivit et al., 1977
Quadrum intermedium Varol, 1992
Genus *Rotelapillus* Noël, 1973
Rotelapillus biarcus (Bukry, 1969) Lees and Bown, 2006
Dinoflagellate cysts
Cyclonephelium compactum-membraniphorum complex Marshall and Batten, 1988
Planktonic foraminifera
Genus *Dicarinella* Porthault, in Donze et al., 1970
Dicarinella canaliculata (Reuss, 1854)
Dicarinella falsohelvetica Desmares, 2020
Dicarinella hagni (Scheibnerova, 1962)
Dicarinella imbricata (Mornod, 1950)
Dicarinella marianosi (Douglas, 1969)
Helvetoglobotruncana helvetica (Bolli, 1945)
Genus *Heterohelix* Ehrenberg, 1843
Laeviella bentonensis (Morrow, 1934)
Marginotruncana cf. *coldreriensis* (Gandolfi, 1957)
Marginotruncana cf. *schneegansi* (Sigal, 1952)
Marginotruncana cf. *sigali* (Reichel, 1950)
Marginotruncana Hofker, 1956
Marginotruncana sigali (Reichel, 1950)
Muricohedbegella delrioensis (Carsey, 1926)
Muricohedbergella kyphoma (Hasegawa, 1999)
Neogloboquadrina incompta (Cifelli, 1961)
Neogloboquadrina pachyderma (Ehrenberg, 1862)
Praeglobotruncana plenusiensis Falzoni and Petrizzo, 2020
Genus *Rotalipora* Brotzen, 1942
Rotalipora cushmani (Morrow, 1934)
Genus *Thalmanninella* Sigal, 1948
Thalmanninella deeckei (Franke, 1925)
Thalmanninella greenhornensis (Morrow, 1934)

Data availability

Data will be made available on request.

References

Adams, D.D., Hurtgen, M.T., Sageman, B.B., 2010. Volcanic triggering of a biogeochemical cascade during Oceanic Anoxic Event 2. Nat. Geosci. 3 (3), 201–204.

Arriaga, M.E., Frija, G., Parente, M., Caus, E., 2016. Benthic Foraminifera in the aftermath of the Cenomanian-Turonian Boundary extinction event in the carbonate platform facies of the Southern Apennines (Italy). J. Foraminiferal Res. 46, 9–24.

Arthur, M.A., Premoli Silva, I., 1982. Development of widespread organic carbon-rich strata in the Mediterranean Tethys. In: Schlanger, S.O., Cita, M.B. (Eds.), Nature of Cretaceous Carbon-Rich Facies. Academic Press, London, pp. 7–54.

Arthur, M.A., Schlanger, S.O., Jenkyns, H.C., 1987. The Cenomanian-Turonian oceanic anoxic event II. Paleoceanographic controls on organic-matter production and preservation. In: Brooks, J., Fleet, A.J. (Eds.), Marine Petroleum Source Rocks. Geological Society, London, Special Publication No. 26, pp. 401–420.

Arthur, M.A., Dean, W.E., Pratt, L.M., 1988. Geochemical and climatic effects of increased marine organic carbon burial at the Cenomanian/Turonian boundary. Nature 335 (6192), 714–717.

Bambach, R.K., 2006. Phanerozoic biodiversity mass extinctions. Annu. Rev. Earth Planet. Sci. 34, 127–155.

Barclay, R.S., McElwain, J.C., Sageman, B.B., 2010. Carbon sequestration activated by a volcanic CO_2 pulse during Ocean Anoxic Event 2. Nat. Geosci. 3 (3), 205–208.

Batenburg, S.J., De Vleeschouwer, D., Sprovieri, M., Hilgen, F.J., Gale, A.S., Singer, B.S., Koeberl, C., Coccioni, R., Claeys, P., Montanari, A., 2016. Orbital control on the timing of oceanic anoxia in the Late Cretaceous. Clim. Past 12 (10), 1995–2009.

Bauer, J., Steuber, T., Kuss, H.-J., 2004. Distribution of shallow-water benthics (rudists, calcareous algae, benthic foraminifera) in the Cenomanian-Turonian carbonate platform sequence of Sinai, Egypt. Courier-Forschungsinstitut Senckenberg 247, 207–231.

Bernoulli, D., 2001. Mesozoic-Tertiary carbonate platforms, slopes and basins of the external Apennines and Sicily. In: Vai, G.B., Martini, I.P. (Eds.), Anatomy of an Orogen: The Apennines and Adjacent Mediterranean Basins. Kluwer Academic Publishers, pp. 307–325.

Berthou, P.Y., 1984. Albian-Turonian stage boundaries and subdivisions in the Western Portuguese basin, with special emphasis on the Cenomanian-Turonian boundary in the ammonite facies and the rudist facies. Bulletin de la Société géologique du Danmark 33, 41–55.

Bice, K.L., Huber, B.T., Norris, R.D., 2003. Extreme polar warmth during the Cretaceous greenhouse? Paradox of the late Turonian $\delta^{18}O$ record at Deep Sea Drilling Project Site 511. Paleoceanography 18 (2), 1031.

Bjerrum, C.J., Bendtsen, J., Legarth, J.J.F., 2006. Modeling organic carbon burial during sea level rise with reference to the Cretaceous. Geochem. Geophys. Geosyst. 7 (5), Q05008.

Blättler, C.L., Jenkyns, H.C., Reynard, L.M., Henderson, G.M., 2011. Significant increases in global weathering during Oceanic Anoxic events 1a and 2 indicated by calcium isotopes. Earth Planet. Sci. Lett. 309 (1–2), 77–88.

Bomou, B., Adatte, T., Tantawy, A.A., Mort, H., Fleitmann, D., Huang, Y., Föllmi, K.B., 2013. The expression of the Cenomanian–Turonian Oceanic Anoxic Event in Tibet. Palaeogeogr. Palaeoclimatol. Palaeoecol. 369, 466–481.

Bosellini, A., 2004. The western passive margin of Adria and its carbonate platforms. In: Special Volume of the Italian Geological Society for the IGC 32-Florence 2004, pp. 79–92.

Boulila, S., Charbonnier, G., Spangenberg, J.E., Gardin, S., Galbrun, B., Briard, J., Le Callonnec, L., 2020. Unraveling short-and long-term carbon cycle variations during the Oceanic Anoxic Event 2 from the Paris Basin Chalk. Glob. Planet. Chang. 186, 103126.

Bowman, A.R., Bralower, T.J., 2005. Paleoceanographic significance of high-resolution carbon isotope records across the Cenomanian–Turonian boundary in the Western Interior and New Jersey coastal plain, USA. Mar. Geol. 217, 305–321.

Bown, P.R., Young, J.R., 1998. Techniques. In: Bown, P.R. (Ed.), Calcareous Nannofossil Biostratigraphy. Chapman and Hall, London, pp. 16–28. https://doi.org/10.1007/978-94-011-4902-0_2.

Bown, P.R., Lees, J.A., Young, J.R., 2004. Calcareous nannoplankton evolution and diversity through time. Coccolithophores: Mol. Process. Global Impact 481–508.

Bralower, T.J., 1988. Calcareous nannofossil biostratigraphy and assemblages of the Cenomanian–Turonian boundary interval: implications for the origin and timing of oceanic anoxia. Paleoceanography 3, 275–316.

Bralower, T.J., Bergen, J.A., 1998. Cenomanian-Santonian calcareous nannofossil biostratigraphy of a transect of cores drilled across the Western Interior Seaway. In: Dean, W.E., Arthur, M.A. (Eds.), Stratigraphy and Paleoenvironments of the Cretaceous Western Interior Seaway. SEPM Concepts in Sedimentology and Paleontology, vol. 6, pp. 59–77.

Bryant, R., Leckie, R.M., Bralower, T.J., Jones, M.M., Sageman, B.B., 2021. Microfossil and geochemical records reveal high-productivity paleoenvironments in the Cretaceous Western Interior Seaway during Oceanic Anoxic Event 2. Palaeogeogr. Palaeoclimatol. Palaeoecol. 584, 110679.

Callapez, P., 2003. The Cenomanian-Turonian transition in West Central Portugal: ammonites and biostratigraphy. Ciências da Terra 15, 53–69.

Caron, M., Homewood, P., 1983. Evolution of early planktic foraminifers. Mar. Micropaleontol. 7 (6), 453–462.

Caron, M., Dall'Agnolo, S., Accarie, H., Barrera, E., Kauffman, E.G., Amédro, F., Robaszynski, F., 2006. High-resolution stratigraphy of the Cenomanian-Turonian boundary interval at Pueblo (USA) and Wadi Bahloul (Tunisia): stable isotope and bio-events correlation. Geobios 39, 171–200.

Chiocchini, M., Farinacci, A., Mancinelli, A., Molinari, V., Potetti, M., 1994. Biostratigrafia a foraminiferi, dasicladali e calpionelle delle successioni carbonatiche mesozoiche dell'Appennino centrale (Italia). In: Mancinelli, A. (Ed.), Biostratigrafia dell'Italia centrale: Studi Geologici Camerti, Volume Speciale, pp. 9–129.

Clarke, L.J., Jenkyns, H.C., 1999. New oxygen isotope evidence for long-term Cretaceous climatic change in the Southern Hemisphere. Geology 27 (8), 699–702.

Clarkson, M.O., Kasemann, S.A., Wood, R.A., Lenton, T.M., Daines, S.J., Richoz, S., Ohnemueller, F., Meixner, A., Poulton, S.W., Tipper, E.T., 2015. Ocean acidification and the Permo-Triassic mass extinction. Science 348, 229–232.

Clarkson, M.O., Stirling, C.H., Jenkyns, H.C., Dickson, A.J., Porcelli, D., Moy, C.M., Pogge von Strandmann, P.A.E., Cooke, I.R., Lenton, T.M., 2018. Uranium isotope evidence for two episodes of deoxygenation during Oceanic Anoxic Event 2. Proc. Natl. Acad. Sci. USA 115, 2918–2923.

Cobban, W.A., 1988. The Upper Cretaceous Ammonite *Watinoceras* Warren in the Western Interior of the United States. U.S. Geol. Den. Surv. Bull. 1788, 1–15.

Cobban, W.A., Scott, G.R., 1972. Stratigraphy and ammonite fauna of the Graneros Shale and Greenhorn Limestone near Pueblo, Colorado (No. 645). United States Geological Survey Professional Paper 645, p. 108.

Consorti, L., Navarro-Ramirez, J.P., Bodin, S., Immenhauser, A., 2018. The architecture and associated fauna of *Perouvianella peruviana*, an endemic larger benthic foraminifera from the Cenomanian-Turonian transition interval of Central Peru. Facies 64, 1–15. https://doi.org/10.1007/s10347-017-0514-z.

Corbett, M.J., Watkins, D.K., Pospichal, J.J., 2014. A quantitative analysis of calcareous nannofossil bioevents of the Late Cretaceous (late Cenomanian-Coniacian) Western Interior Seaway and their reliability in established zonation schemes. Mar. Micropaleontol. 109, 30–45.

Crumière, J.P., 1990. Crise anoxique à la limite Cénomanien-Turonien dans le bassin subalpin oriental (Sud-Est de la France). Relation avec l'eustatisme. Geobios Mémoire Spécial 11, 189–203.

De Castro, P., Sirna, G., 1996. *Durania arnaudi* biostrome of El-Hassana, Abu Roash area, Egypt. Geol. Romana 32, 69–91.

Desmares, D., Grosheny, D., Beaudoin, B., Gardin, S., Gauthier-Lafaye, F., 2007. High resolution stratigraphic record constrained by volcanic ashes layers at the Cenomanian-Turonian boundary in the Western Interior Basin, USA. Cretac. Res. 28, 561–582.

Desmares, D., Crognier, N., Bardin, J., Testé, M., Beaudoin, B., Grosheny, D., 2016. A new proxy for Cretaceous paleoceanographic and paleoclimatic reconstructions: Coiling direction changes in the planktonic foraminifera *Muricohedbergella delrioensis*. Palaeogeogr. Palaeoclimatol. Palaeoecol. 445, 8–17.

Desmares, D., Testé, M., Broche, B., Tremblin, M., Gardin, S., Villier, L., Masure, E., Grosheny, D., Morel, N., Raboeuf, P., 2020. High-resolution biostratigraphy and chemostratigraphy of the Cenomanian stratotype area (Le Mans, France). Cretac. Res. 106 (104198), 1–15.

Dodsworth, P., 2000. Trans-Atlantic dinoflagellate cyst stratigraphy across the Cenomanian-Turonian (Cretaceous) Stage boundary. J. Micropalaeontol. 19, 69–84.

Doo, S.S., Fujita, K., Byrne, M., Uthicke, S., 2014. Fate of calcifying tropical symbiont-bearing Large Benthic Foraminifera: living sands in a changing ocean. Biol. Bull. 226, 169–186.

Du Vivier, A.D.C., Selby, D., Sageman, B.B., Jarvis, I., Gröcke, D.R., Voigt, S., 2014. Marine $^{187}Os/^{188}Os$ isotope stratigraphy reveals the interaction of volcanism and ocean circulation during Oceanic Anoxic Event 2. Earth Planet. Sci. Lett. 389, 23–33.

Du Vivier, A.D.C., Jacobson, A.D., Lehn, G.O., Selby, D., Hurtgen, M.T., Sageman, B.B., 2015. Ca isotope stratigraphy across the Cenomanian-Turonian OAE 2: Links between volcanism, seawater geochemistry, and the carbonate fractionation factor. Earth Planet. Sci. Lett. 416, 121–131. https://doi.org/10.1016/j.epsl.2015.02.001.

Eicher, D.L., 1969. Paleobathymetry of Cretaceous Greenhorn Sea in eastern Colorado. AAPG Bull. 53 (5), 1075–1090.

Eicher, D.L., Diner, R., 1985. Foraminifera as indicators of water mass in the Cretaceous Greenhorn Sea, Western Interior. In: Pratt, L.M., Kauffman, E.G., Zelt, F.B. (Eds.), Fine-Grained Deposits and Biofacies of the Cretaceous Western Interior Seaway: Evidence of Cyclic Sedimentary Processes, Field Trip Guidebook, Society of Economic Paleontologists and Mineralogists, vol. 4, pp. 60–71.

Eicher, D.L., Worstell, P., 1970. Cenomanian and Turonian foraminifera from the Great Plains, United States. Micropaleontology 16, 269–324.

Elderbak, K., Leckie, R.M., 2016. Paleocirculation and foraminiferal assemblages of the Cenomanian-Turonian Bridge Creek Limestone bedding couplets: Productivity vs. dilution during OAE 2. Cretac. Res. 60, 52–77.

Elderbak, K., Leckie, R.M., Tibert, N.E., 2014. Paleoenvironmental and paleoceanographic changes across the Cenomanian-Turonian Boundary Event (Oceanic Anoxic Event 2) as indicated by foraminiferal assemblages from the eastern margin of the Cretaceous Western Interior Sea. Palaeogeogr. Palaeoclimatol. Palaeoecol. 413, 29–48.

Eldrett, J.S., Minisini, D., Bergman, S.C., 2014. Decoupling of the carbon cycle during Ocean Anoxic Event 2. Geology 42, 567–570.

Eldrett, J.S., Ma, C., Bergman, S.C., Lutz, B., Gregory, F.J., Dodsworth, P., Phipps, M., Hardas, P., Minisini, D., Ozkan, A., Ramezani, J., Bowring, S.A., Kamo, S.L., Ferguson, K., Macaulay, C., Kelly, A.E., 2015. An astronomically calibrated stratigraphy of the Cenomanian, Turonian and earliest Coniacian from the Cretaceous Western Interior Seaway, USA: Implications for global chronostratigraphy. Cretac. Res. 56, 316–344.

Eldrett, J.S., Dodsworth, P., Bergman, S.C., Wright, M., Minisini, D., 2017. Water-mass evolution in the Cretaceous Western Interior Seaway of North America and equatorial Atlantic. Clim. Past 13, 855–878.

Erba, E., 2004. Calcareous nannofossils and Mesozoic oceanic anoxic events. Mar. Micropaleontol. 52, 85–106. https://doi.org/10.1016/j.marmicro.2004.04.007.

Erba, E., Parente, M., 2024. The resilience of Tethyan planktonic and benthic calcifying algae to Early Cretaceous perturbations: Comparison between the Valanginian Weissert Event and the early Aptian Oceanic Anoxic Event 1a. In: Hart, M.B., Batenburg, S.J., Huber, B.T., Price, G.D., Thibault, N., Wagreich, M., Walaszczyk, I. (Eds.), Cretaceous Project 200 Volume 2: Regional Studies. Geological Society, London. https://doi.org/10.1144/SP545-2023-125. Special Publications 545.

Erba, E., Tremolada, F., 2004. Nannofossil carbonate fluxes during the Early Cretaceous: phytoplankton response to nutrification episodes, atmospheric CO_2, and anoxia. Paleoceanography 19, PA1008. https://doi.org/10.1029/2003PA000884.

Erba, E., Bottini, C., Weissert, H.J., Keller, C.E., 2010. Calcareous nannoplankton response to surface-water acidification around Oceanic Anoxic Event 1a. Science 329, 428–432. https://doi.org/10.1126/science.1188886.

Erbacher, J., Thurow, J., Littke, R., 1996. Evolution patterns of radiolaria and organic matter variations: a new approach to identify sea-level changes in mid-Cretaceous pelagic environments. Geology 24, 499–502.

Erbacher, J., Friedrich, O., Wilson, P.A., Birch, H., Mutterlose, J., 2005. Stable organic carbon isotope stratigraphy across Oceanic Anoxic Event 2 of Demerara rise, western tropical Atlantic. Geochem. Geophys. Geosyst. 6, Q06010. https://doi.org/10.1029/2004GC000850.

Falzoni, F., Petrizzo, M.R., 2020. Patterns of planktonic foraminiferal extinctions and eclipses during Oceanic Anoxic Event 2 at Eastbourne (SE England) and other mid-low latitude locations. Cretac. Res. 116, 104593.

Falzoni, F., Petrizzo, M.R., 2022. Evidence for changes in sea-surface circulation patterns and ~20°N equatorward expansion of the Boreal bioprovince during a cold snap of Oceanic Anoxic Event 2 (Late Cretaceous). Glob. Planet. Chang. 208, 103678. https://doi.org/10.1016/j.gloplacha.2021.103678.

Falzoni, F., Petrizzo, M.R., Jenkyns, H.C., Gale, A.S., Tsikos, H., 2016. Planktonic foraminiferal biostratigraphy and assemblage composition across the Cenomanian-Turonian boundary interval at Clot Chevalier (Vocontian Basin, SE France). Cretac. Res. 59, 69–97.

Falzoni, F., Petrizzo, M.R., Caron, M., Leckie, R.M., Elderbak, K., 2018a. Age and synchronicity of planktonic foraminiferal bioevents across the Cenomanian-Turonian boundary interval (Late Cretaceous). Newsl. Stratigr. 51, 343–380.

Falzoni, F., Petrizzo, M.R., Valagussa, M., 2018b. A morphometric methodology to assess planktonic foraminiferal response to environmental perturbations: the case study of Oceanic Anoxic Event 2, Late Cretaceous. Boll. Soc. Paleontol. Ital. 57, 103–124.

Faucher, G., Erba, E., Bottini, C., Gambacorta, G., 2017. Calcareous nannoplankton response to the latest Cenomanian Oceanic Anoxic Event 2 perturbation. Riv. Ital. Paleontol. Stratigr. 123 (1), 159–176.

Finnegan, S., Anderson, S.C., Harnik, P.G., Simpson, C., Tittensor, D.P., Byrnes, J.E., Finkel, Z.V., Lindberg, D.R., Liow, L.H., Lockwood, R., Lotze, H.K., McClain, C.R., McGuire, J.L., O'Dea, A., Pandolfi, J.M., 2015. Paleontological baselines for evaluating extinction risk in the modern oceans. Science 348, 567–570.

Fleury, J.J., 1971. Le Cénomanien a foraminifères benthoniques du Massif du Varassova (Zone du Gavrovo, Akarnanie, Grèce continentale). Rev. Micropaleontol. 14, 181–194.

Fleury, E., Barbier, P., Petton, B., Normand, J., Thomas, Y., Pouvreau, S., Daigle, G., Pernet, F., 2020. Latitudinal drivers of oyster mortality: deciphering host, pathogen and environmental risk factors. Sci. Rep. 10, 7264. https://doi.org/10.1038/s41598-020-64086-1.

Forster, A., Schouten, S., Moriya, K., Wilson, P.A., Sinninghe Damsté, J.S., 2007. Tropical warming and intermittent cooling during the Cenomanian/Turonian oceanic anoxic event 2: Sea surface temperature records from the equatorial Atlantic. Paleoceanography 22, PA1219. https://doi.org/10.1029/2006PA001349.

Friedrich, O., Erbacher, J., Mutterlose, J., 2006. Paleoenvironmental changes across the Cenomanian-Turonian boundary event (Oceanic Anoxic Event 2) as indicated by benthic foraminifera from the Demerara rise (ODP Leg 207). Rev. Micropaleontol. 49 (3), 121–139.

Friedrich, O., Norris, R.D., Erbacher, J., 2012. Evolution of middle to Late Cretaceous oceans—a 55 my record of Earth's temperature and carbon cycle. Geology 40 (2), 107–110.

Frijia, G., Parente, M., 2008. Strontium isotope stratigraphy in the upper Cenomanian shallow-water carbonates of the southern Apennines: short-term perturbations of marine $^{87}Sr/^{86}Sr$ during the oceanic anoxic event 2. Palaeogeogr. Palaeoclimatol. Palaeoecol. 261, 15–29. https://doi.org/10.1016/j.palaeo.2008.01.003.

Frijia, G., Parente, M., Di Lucia, M., Mutti, M., 2015. Carbon and strontium isotope stratigraphy of the Upper Cretaceous (Cenomanian-Campanian) shallow-water carbonates of southern Italy: Chronostratigraphic calibration of larger foraminifera biostratigraphy. Cretac. Res. 53, 110–139. https://doi.org/10.1016/j.cretres.2014.11.002.

Frijia, G., Forkner, R., Minisini, D., Pacton, M., Struck, U., Mutti, M., 2019. Cyanobacteria proliferation in the Cenomanian-Turonian Boundary Interval of the Apennine Carbonate Platform: Immediate response to the environmental perturbations associated with OAE-2? Geochem. Geophys. Geosyst. 20, 2698–2716. https://doi.org/10.1029/2019GC008306.

Fujita, K., Okai, T., Hosono, T., 2014. Oxygen metabolic responses of three species of large Benthic Foraminifers with algal symbionts to temperature stress. PLoS One 9, e90304.

Gale, A.S., Christensen, W.K., 1996. Occurrence of the belemnite *Actinocamax plenus* in the Cenomanian of SE France and its significance. Bull. Geol. Soc. Den. 43, 68–77.

Gale, A.S., Jenkyns, H.C., Kennedy, W.J., Corfield, R.M., 1993. Chemostratigraphy versus biostratigraphy: data from around the Cenomanian-Turonian boundary. J. Geol. Soc. Lond. 150 (1), 29–32.

Gale, A.S., Smith, A.B., Monks, N.E.A., Young, J.A., Howard, A., Wray, D.S., Huggett, J. M., 2000. Marine biodiversity through the late Cenomanian-early Turonian: palaeoceanographic controls and sequence stratigraphic biases. J. Geol. Soc. Lond. 157, 745–757.

Gale, A.S., Kennedy, W.J., Voigt, S., Walaszczyk, I., 2005. Stratigraphy of the upper Cenomanian-lower Turonian Chalk succession at Eastbourne, Sussex, UK: Ammonites, inoceramid bivalves and stable carbon isotopes. Cretac. Res. 26, 460–487.

Gale, A.S., Jenkyns, H.C., Tsikos, H., van Breugel, Y., Sinninghe Damsté, J.S., Bottini, C., Erba, E., Russo, F., Falzoni, F., Petrizzo, M.R., Dickson, A.J., Wray, D.S., 2019. High-resolution bio- and chemostratigraphy of an expanded record of Oceanic Anoxic Event 2 (late Cenomanian-early Turonian) at Clot Chevalier, near Barrême, SE

France (Vocontian Basin, SE France). Newsl. Stratigr. 52, 97–129. https://doi.org/10.1127/nos/2018/0445.
Gambacorta, G., Jenkyns, H.C., Russo, F., Tsikos, H., Wilson, P.A., Faucher, G., Erba, E., 2015. Carbon-and oxygen-isotope records of mid-Cretaceous Tethyan pelagic sequences from the Umbria–Marche and Belluno Basins (Italy). Newsl. Stratigr. 48 (3), 299–323.
Gangl, S.K., Moy, C.M., Stirling, C.H., Jenkyns, H.C., Crampton, J.S., Clarkson, M.O., Ohneiser, C., Porcelli, D., 2019. High-resolution records of Oceanic Anoxic Event 2: insights into the timing, duration and extent of environmental perturbations from the palaeo-South Pacific Ocean. Earth Planet. Sci. Lett. 518, 172–182.
Gavrilov, Yu.O., Shcherbinina, E.A., Golovanova, O.V., Pokrovsky, B.G., 2013. The late Cenomanian paleoecological event (OAE 2) in the eastern Caucasus basin of northern Peri-Tethys. Lithol. Miner. Resour. 6, 457–488.
Gertsch, B., Adatte, T., Keller, G., Tantawi, A.A.A.M., Berner, Z., Mort, H.P., Fleitmann, D., 2010. Middle and late Cenomanian oceanic anoxic events in shallow and deeper shelf environments of western Morocco. Sedimentology 57, 1430–1462. https://doi.org/10.1111/j.1365-3091.2010.
Gili, E., Götz, S., 2018. Part N, revised, volume 1, chapter 26B: Paleoecology of Rudists. Treatise Online 103, 1–29.
Greene, S.E., Martindale, R.C., Ritterbush, K.A., Bottjer, D.J., Corsetti, F.A., Berelson, W. M., 2012. Recognising ocean acidification in deep time: an evaluation of the evidence for acidification across the Triassic-Jurassic boundary. Earth Sci. Rev. 113, 72–93.
Grosheny, D., Ferry, S., Lecuyer, C., Thomas, A., Desmares, D., 2017. The Cenomanian–Turonian Boundary Event (CTBE) on the southern slope of the Subalpine Basin (SE France) and its bearing on a probable tectonic pulse on a larger scale. Cretac. Res. 72, 39–65.
Hallock, P., 1985. Why are larger Foraminifera large? Paleobiology 11, 195–208.
Hallock, P., 2000. Symbiont-bearing foraminifera: harbingers of global change? Micropaleontology 46 (1), 95–104.
Hallock, P., Talge, H.K., Smith, K., Cockey, E.M., 1993. Bleaching in a reef-dwelling Foraminifera *Amphistegina gibbosa*. In: Proceedings Seventh International Coral Reef Symposium, Guam, June 1992, 1, pp. 44–49.
Hardas, P., Mutterlose, J., 2006. Calcareous nannofossil biostratigraphy of the Cenomanian/Turonian boundary interval of ODP Leg 207 at the Demerara rise. Rev. Micropaleontol. 49, 165–179.
Harries, P.J., Little, C.T.S., 1999. The early Toarcian (Early Jurassic) and the Cenomanian–Turonian (Late Cretaceous) mass extinctions; similarities and contrasts. Palaeogeogr. Palaeoclimatol. Palaeoecol. 154, 39–66.
Hart, M.B., 1999. The evolution and biodiversity of Cretaceous planktonic Foraminiferida. Geobios 32, 247–255.
Hart, M.B., Dodsworth, P., Ditchfield, P.W., Duane, A.M., Orth, C.J., 1991. The late Cenomanian event in eastern England. Hist. Biol. 5 (2–4), 339–354.
Hart, M.B., Monteiro, J.F., Watkinson, M.P., Price, G.D., 2002. Correlation of events at the Cenomanian/Turonian boundary: Evidence from Southern England and Colorado. In: Wagreich, M. (Ed.), Aspects of Cretaceous Stratigraphy and Palaeobiogeography. Schriftenreihe der erdwissenschaftliche Kommission der Österreichische Akademie der Wissenschaften15. Verlag der Österreichische Akademie der Wissenschaften, Wien, pp. 35–46.
Hay, W.W., DeConto, R., Wold, C.N., Wilson, K.M., Voigt, S., Schulz, M., Wold-Rossby, A., Dullo, W.C., Ronov, A.B., Balukhovsky, A.N., Soeding, E., 1999. Alternative global Cretaceous paleogeography. In: Barrera, E., Johnson, C.C. (Eds.), The Evolution of the Cretaceous Ocean/Climate System, 332. Geological Society of America Special Paper, Boulder, Colorado, pp. 1–47.
Henehan, M.J., Ridgwell, A., Thomas, E., Zhang, S., Alegret, L., Schmidt, D.N., Rae, J.W. B., Witts, J.D., Landman, N.H., Greene, S.E., Huber, B.T., Super, J.R., Planavsky, N. J., Hull, P.M., 2019. Rapid ocean acidification and protracted Earth system recovery followed the end-Cretaceous Chicxulub impact. Proc. Natl. Acad. Sci. 44, 201905989.
Hernandis, S., Ibarrola, I., Tena-Medialdea, J., Albentosa, M., Prado, P., Vázquez-Luis, M., García-March, J.R., 2023. Physiological responses of the fan mussel *Pinna nobilis* to temperature: ecological and captivity implications. Mediterr. Mar. Sci. 24 (2), 259–271. https://doi.org/10.12681/mms.31050.
Higgins, M.B., Robinson, R.S., Husson, J.M., Carter, S.J., Pearson, A., 2012. Dominant eukaryotic export production during ocean anoxic events reflects the importance of recycled NH4+. Proc. Natl. Acad. Sci. 109 (7), 2269–2274.
Hönisch, B., Ridgwell, A., Schmidt, D.N., Thomas, E., Gibbs, S.J., Sluijs, A., Zeebe, R., Kump, L., Martindale, R.C., Greene, S.E., Kiessling, W., Ries, J., Zachos, J.C., Royer, D.L., Barker, S., Marchitto, T.M., Moyer, R., Pelejero, C., Ziveri, P., Foster, G. L., Williams, B., 2012. The geological record of ocean acidification. Science 335, 1058–1063.
Hottinger, L., 1982. Larger Foraminifera, Giant Cells with a Historical Background. Naturwissenschaften 69, 361–371.
Huber, B.T., Petrizzo, M.R., 2014. Evolution and taxonomic study of the Cretaceous planktic foraminiferal genus *Helvetoglobotruncana* Reiss, 1957. J. Foraminiferal Res. 44 (1), 40–57.
Huber, B.T., Leckie, R.M., Norris, R.D., Bralower, T.J., CoBabe, E., 1999. Foraminiferal assemblage and stable isotopic change across the Cenomanian-Turonian boundary in the subtropical North Atlantic. J. Foraminifer. Res. 29, 392–417.
Huber, B.T., Norris, R.D., MacLeod, K.G., 2002. Deep-sea paleotemperature record of extreme warmth during the Cretaceous. Geology 30 (2), 123–126.
Huber, B.T., Petrizzo, M.R., Young, J.R., Falzoni, F., Gilardoni, S.E., Bown, P.R., Wade, B. S., 2016. Pforams@mikrotax: a new online taxonomic database for planktonic foraminifera. Micropaleontology 62 (6), 429–438.
Huber, B.T., MacLeod, K.G., Watkins, D.K., Coffin, M.F., 2018. The rise and fall of the Cretaceous Hot Greenhouse climate. Glob. Planet. Chang. 167, 1–23.
Iwasaki, S., Kimoto, K., Okazaki, Y., Ikehara, M., 2019. Micro-CT scanning of tests of three Planktic Foraminiferal species to clarify dissolution process and progress. Geochem. Geophys. Geosyst. 20 (12), 6051–6065.
Jarvis, I., Gale, A.S., Jenkyns, H.C., Pearce, M.A., 2006. Secular variation in Late Cretaceous carbon isotopes and sea-level change: evidence from a new $\delta^{13}C$ carbonate reference curve for the Cenomanian-Campanian (99.6-70.6 Ma). Geol. Mag. 143 (5), 561–608. https://doi.org/10.1017/S0016756806002421.
Jarvis, I., Lignum, J.S., Gröcke, D.R., Jenkyns, H.C., Pearce, M.A., 2011. Black shale deposition, atmospheric CO_2 drawdown, and cooling during the Cenomanian-Turonian Oceanic Anoxic Event. Paleoceanography 26, PA3201. https://doi.org/10.1029/2010PA002081.
Jeans, C.V., Wray, D.S., Williams, C.T., Bland, D.J., Wood, C.J., 2021. Redox conditions, glacio-eustasy, and the status of the Cenomanian–Turonian Anoxic Event: new evidence from the Upper Cretaceous Chalk of England. Acta Geol. Pol. 71, 1–50. https://doi.org/10.24425/agp.2020.134556.
Jefferies, R.P.S., 1962. The palaeoecology of the *Actinocamax plenus* subzone (lowest Turonian) in the Anglo-Paris Basin. Palaeontology 4, 609–647.
Jefferies, R.P.S., 1963. The stratigraphy of the *Actinocamax plenus* subzone (Turonian) in the Anglo-Paris Basin. Proc. Geol. Assoc. 74, 1–33.
Jenkyns, H.C., 2003. Evidence for rapid climate change in the Mesozoic–Palaeogene greenhouse world. Philos. Trans. R. Soc. London, Ser. A 361 (1810), 1885–1916.
Jenkyns, H.C., 2010. Geochemistry of oceanic anoxic events. Geochem. Geophys. Geosyst. 11, Q03004. https://doi.org/10.1029/2009GC002788.
Jenkyns, H.C., Gale, A.S., Corfield, R.M., 1994. Carbon-and oxygen-isotope stratigraphy of the English Chalk and Italian Scaglia and its palaeoclimatic significance. Geol. Mag. 131 (1), 1–34.
Jenkyns, H.C., Dickson, A.J., Ruhl, M., Boorn, S.H., 2017. Basalt-seawater interaction, the Plenus Cold Event, enhanced weathering and geochemical change: Deconstructing Oceanic Anoxic Event 2 (Cenomanian–Turonian, Late Cretaceous). Sedimentology 64, 16–43.
Jones, M.M., Sageman, B.B., Selby, D., Jicha, B.R., Singer, B.S., Titus, A.L., 2021. Regional chronostratigraphic synthesis of the Cenomanian-Turonian Oceanic Anoxic Event 2 (OAE2) interval, Western Interior Basin (USA): New Re-Os chemostratigraphy and $^{40}Ar/^{39}Ar$ geochronology. GSA Bull. 133 (5–6), 1090–1104.
Jones, M.M., Sageman, B.B., Selby, D., Jacobson, A.D., Batenburg, S.J., Riquier, L., MacLeod, K.G., Huber, B.T., Bogus, K.A., Tejada, M.L.G., Kuroda, J., Hobbs, R.W., 2023. Abrupt episode of mid-Cretaceous ocean acidification triggered by massive volcanism. Nat. Geosci. 16 (2), 169–174.
Jurikova, H., Gutjahr, M., Wallmann, K., Fögel, S., Liebetrau, V., Posenato, R., Angiolini, L., Garbelli, C., Brand, U., Wiedenbeck, M., Eisenhauer, A., 2020. Permian–Triassic mass extinction pulses driven by major marine carbon cycle perturbations. Nat. Geosci. 13, 745–750. https://doi.org/10.1038/s41561-020-00646-4.
Kalanat, B., Vaziri-Moghaddam, H., 2019. The Cenomanian/Turonian boundary interval deep-sea deposits in the Zagros Basin (SW Iran): Bioevents, carbon isotope record and palaeoceanographic model. Palaeogeogr. Palaeoclimatol. Palaeoecol. 533, 109238.
Kalanat, B., Mahmudy-Gharaie, M.H., Vahidinia, M., Vaziri-Moghaddam, H., Kano, A., Kumon, F., 2018. Paleoenvironmental perturbation across the Cenomanian/Turonian boundary of the Kopet-Dagh Basin (NE Iran), inferred from geochemical anomalies and benthic foraminiferal assemblages. Cretac. Res. 86, 261–275.
Kauffman, E.G., Johnson, C.C., 1988. The morphological and ecological evolution of middle and Upper Cretaceous reef-building rudistids. Palaios 3, 194–216.
Kawahata, H., Fujita, K., Iguchi, A., Inoue, M., Iwasaki, S., Kuroyanagi, A., Maeda, A., Manaka, T., Moriya, K., Takagi, H., Toyofuku, T., Yoshimura, T., Suzuki, A., 2019. Perspective on the response of marine calcifiers to global warming and ocean acidification—Behavior of corals and foraminifera in a high CO_2 world "hot house". Prog Earth Planet Sci 6, 5. https://doi.org/10.1186/s40645-018-0239-9.
Keller, G., Pardo, A., 2004. Age and paleoenvironment of the Cenomanian-Turonian global stratotype section and point at Pueblo, Colorado. Mar. Micropaleontol. 51, 95–128.
Keller, G., Han, Q., Adatte, T., Burns, S., 2001. Paleoenvironment of the Cenomanian-Turonian transition at Eastbourne, England. Cretac. Res. 22, 391–422.
Keller, G., Berner, Z., Adatte, T., Stueben, D., 2004. Cenomanian–Turonian and $\delta^{13}C$, and $\delta^{18}O$, sea level and salinity variations at Pueblo, Colorado. Palaeogeogr. Palaeoclimatol. Palaeoecol. 211, 19–43.
Keller, G., Adatte, T., Berner, Z., Chellai, E.H., Stueben, D., 2008. Oceanic events and biotic effects of the Cenomanian-Turonian anoxic event, Tarfaya Basin, Morocco. Cretac. Res. 29, 976–994.
Kemp, D.B., Eichenseer, K., Kiessling, W., 2015. Maximum rates of climate change are systematically underestimated in the geological record. Nat. Commun. 6 (1), 8890.
Kennedy, W.J., Cobban, W.A., 1991. Stratigraphy and interregional correlation of the Cenomanian–Turonian transition in the Western Interior of the United States near Pueblo, Colorado, a potential boundary stratotype for the base of the Turonian Stage. Newsl. Stratigr. 24, 1–33.
Kennedy, W.J., Cobban, W.A., Elder, W.P., Kirkland, J.I., 1999. Lower Turonian (Upper Cretaceous) *Watinoceras devonense* Zone ammonite fauna in Colorado, USA. Cretac. Res. 20, 629–639.
Kennedy, W.J., Walaszczyk, I., Cobban, W.A., 2000. Pueblo, Colorado, USA, Candidate Global Boundary Stratotype Section and Point for the base of the Turonian stage of the Cretaceous and for the middle Turonian substage, with a revision of the Inoceramidae (Bivalvia). Acta Geol. Pol. 50, 295–334.
Kennedy, W.J., Walaszczyk, I., Cobban, W.A., 2005. The Global Boundary Stratotype Section and Point for the base of the Turonian Stage of the Cretaceous: Pueblo, Colorado, USA. Episodes 28, 93–104.

Kerr, A.C., 1998. Oceanic plateau formation: a cause of mass extinction and black shale deposition around the Cenomanian–Turonian boundary? J. Geol. Soc. Lond. 155 (4), 619–626.
Kiessling, W., Simpson, C., 2010. On the potential for ocean acidification to be a general cause of ancient reef crises. Glob. Chang. Biol. 17, 56–67.
Kinoshita, S., Kuroyanagi, A., Kawahata, H., Fujita, K., Ishimura, T., Suzuki, A., Sasaki, O., Nishi, H., 2021. Temperature effects on the shell growth of a larger benthic foraminifer (*Sorites orbiculus*): results from culture experiments and micro X-ray computed tomography. Mar. Micropaleontol. 163, 101960.
Kitch, G.D., Jacobson, A.D., Sageman, B.B., Coccioni, R., Chung-Swanson, T., Ankney, M. E., Hurtgen, M.T., 2022. Calcium isotope ratios of malformed foraminifera reveal biocalcification stress preceded Oceanic Anoxic Event 2. Commun. Earth Environ. 3 (1), 315.
Křížová, B.B., Consorti, L., Cardelli, S., Schmitt, K.E., Brombin, V., Franceschi, M., Tunis, G., Bonini, L., Frijia, G., 2024. Late Cretaceous (Cenomanian-Turonian) temperature evolution and biotic response in the Adriatic Carbonate Platform region of Friuli, Northeast Italy. Palaeogeogr. Palaeoclimatol. Palaeoecol. 637, 111995.
Kuhnt, W., Holbourn, A.E., Beil, S., Aquit, M., Krawczyk, T., Flögel, S., Chellai, E.H., Jabour, H., 2017. Unraveling the onset of Cretaceous Oceanic Anoxic Event 2 in an extended sediment archive from the Tarfaya-Laayoune Basin, Morocco. Paleoceanography 32, 923–946.
Kuroda, J., Ohkouchi, N., 2006. Implication of spatiotemporal distribution of black shales deposited during the Cretaceous Oceanic Anoxic Event-2. Paleontol. Res. 10, 345–358.
Kuroda, J., Ogawa, N.O., Tanimizu, M., Coffin, M.F., Tokuyama, H., Kitazato, H., Ohkouchi, N., 2007. Contemporaneous massive subaerial volcanism and Late Cretaceous Oceanic Anoxic Event 2. Earth Planet. Sci. Lett. 256 (1–2), 211–223.
Kuypers, M.M., Pancost, R.D., Damsté, J.S.S., 1999. A large and abrupt fall in atmospheric CO_2 concentration during Cretaceous times. Nature 399 (6734), 342–345.
Kuypers, M.M., Pancost, R.D., Nijenhuis, I.A., Sinninghe Damsté, J.S.S., 2002. Enhanced productivity led to increased organic carbon burial in the euxinic North Atlantic basin during the late Cenomanian oceanic anoxic event. Paleoceanography 17 (4), 3–1.
Lamolda, M.A., Gorostidi, A., Paul, C.R.C., 1994. Quantitative estimates of calcareous nannofossil changes across the Plenus Marls (latest Cenomanian), Dover, England: implications for the generation of the Cenomanian-Turonian Boundary Event. Cretac. Res. 15, 143–164.
Larson, R.L., 1991. Latest pulse of Earth: evidence for a mid-Cretaceous superplume. Geology 19, 547–550.
Larson, R.L., Erba, E., 1999. Onset of the mid-Cretaceous greenhouse in the Barremian-Aptian: Igneous events and the biological, sedimentary, and geochemical responses. Paleoceanography 14 (6), 663–678.
Leckie, R.M., 1985. Foraminifera of the Cenomanian–Turonian boundary interval, Greenhorn Formation, Rock Canyon Anticline, Pueblo, Colorado. In: Pratt, L.M., Kauffman, E.G., Zelt, F.B. (Eds.), Fine-Grained Deposits and Biofacies of the Cretaceous Western Interior Seaway: Evidence of Cyclic Sedimentary Processes, Field Trip Guidebook, Society of Economic Paleontologists and Mineralogists, vol. 4, pp. 139–149.
Leckie, R.M., 1987. Paleoecology of mid-Cretaceous planktonic foraminifera: a comparison of open oceans and epicontinental sea assemblages. Micropaleontology 33, 164–176.
Leckie, R.M., Yuretrich, R.F., West, O.L.O., Finkelstein, D., Schmidt, M., 1998. Paleoceanography of the southwestern Western Interior Sea during the time of the Cenomanian/Turonian boundary (Late Cretaceous). In: Dean, W., Arthur, M.A. (Eds.), Stratigraphy and Paleoenvironments of the Cretaceous Western Interior Seaway. SEPM Concepts in Sedimentology and Paleontology, vol. 6, pp. 101–126.
Leckie, R.M., Bralower, T.J., Cashman, R., 2002. Oceanic anoxic events and plankton evolution: Biotic response to tectonic forcing during the mid-Cretaceous. Paleoceanography 17. https://doi.org/10.1029/2001PA000623.
Li, Y.X., Montañez, I.P., Liu, Z., Ma, L., 2017. Astronomical constraints on global carbon-cycle perturbation during Oceanic Anoxic Event 2 (OAE2). Earth Planet. Sci. Lett. 462, 35–46.
Linnert, C., Mutterlose, J., Erbacher, J., 2010. Calcareous nannofossils of the Cenomanian-Turonian boundary interval from the Boreal Realm (Wunstorf, Northwest Germany). Mar. Micropaleontol. 74, 38–58.
Linnert, C., Mutterlose, J., Mortimore, R., 2011. Calcareous nannofossils from Eastbourne (Southeastern England) and the paleoceanography of the Cenomanian-Turonian boundary interval. Palaios 26 (5), 298–313.
Linnert, C., Robinson, S.A., Lees, J.A., Bown, P.R., Pérez-Rodríguez, I., Petrizzo, M.R., Falzoni, F., Littler, K., Arz, J.A., Russell, E.E., 2014. Evidence for global cooling in the Late Cretaceous. Nat. Commun. 5 (1), 4194.
MacLeod, K.G., Martin, E.E., Blair, S.W., 2008. Nd isotopic excursion across Cretaceous Ocean Anoxic Event 2 (Cenomanian-Turonian) in the tropical North Atlantic. Geology 36 (10), 811–814.
MacLeod, K.G., Huber, B.T., Jiménez Berrocoso, A., Wendler, I., 2013. A stable and hot Turonian without glacial $\delta^{18}O$ excursions is indicated by exquisitely preserved Tanzanian foraminifera. Geology 41 (10), 1083–1086. https://doi.org/10.1130/G34510.1.
Martin, E.E., MacLeod, K.G., Jiménez Berrocoso, A., Bourbon, E., 2012. Water mass circulation on Demerara rise during the Late Cretaceous based on Nd isotopes. Earth Planet. Sci. Lett. 327–328, 111–120. https://doi.org/10.1016/j.epsl.2012.01.037.
McKinney, M.L., 1997. How do rare species avoid extinction? A paleontological view. In: Kunin, W.E., Gaston, K.J. (Eds.), The Biology of Rarity. Population and Community Biology Series 17. Springer, Dordrecht, pp. 110–129. https://doi.org/10.1007/978-94-011-5874-9_7.
Meyers, S.R., Siewert, S.E., Singer, B.S., Sageman, B.B., Condon, D.J., Obradovich, J.D., Jicha, B.R., Sawyer, D.A., 2012. Intercalibration of radioisotopic and astrochronologic time scales for the Cenomanian-Turonian boundary interval, Western Interior Basin, USA. Geology 40 (1), 7–10.
Mitchell, S.F., 2023. The Cretaceous carbonate platforms of the Americas and their rudist bivalves. In: Hart, M.B., Batenburg, S.J., Huber, B.T., Price, G.D., Thibault, N., Wagreich, M., Walaszczyk, I. (Eds.), Cretaceous Project 200 Volume 1: the Cretaceous World. Geological Society, London (Special Publications 544).
Mitchell, R.N., Bice, D.M., Montanari, A., Cleaveland, L.C., Christianson, K.T., Coccioni, R., Hinnov, L.A., 2008. Oceanic anoxic cycles? Orbital prelude to the Bonarelli Level (OAE 2). Earth Planet. Sci. Lett. 267 (1–2), 1–16.
Monteiro, F.M., Pancost, R.D., Ridgwell, A., Donnadieu, Y., 2012. Nutrients as the dominant control on the spread of anoxia and euxinia across the Cenomanian-Turonian oceanic anoxic event (OAE2): Model-data comparison. Paleoceanography 27 (4). https://doi.org/10.1029/2012PA002351.
Morel, L., 1998. Stratigraphie haute résolution du passage Cénomanien-Turonien. Ph.D. thesis. Université Pierre et Marie Curie, Paris, p. 224. VI, (unpublished)s.
Moriya, K., Wilson, P.A., Friedrich, O., Erbacher, J., Kawahata, H., 2007. Testing for ice sheets during the mid-Cretaceous greenhouse using glassy foraminiferal calcite from the mid-Cenomanian tropics on Demerara rise. Geology 35 (7), 615–618.
Mort, H., Jacquat, O., Adatte, T., Steinmann, P., Föllmi, K., Matera, V., Berner, Z., Stüben, D., 2007. The Cenomanian/Turonian anoxic event at the Bonarelli Level in Italy and Spain: enhanced productivity and/or better preservation? Cretac. Res. 28, 597–612.
Moy, A.D., Howard, W.R., Bray, S.G., Trull, T.W., 2009. Reduced calcification in modern Southern Ocean planktonic foraminifera. Nat. Geosci. 2 (4), 276–280.
Müller, T., Jurikova, H., Gutjahr, M., Tomašových, A., Schlögl, J., Liebetrau, L.V., Duarte, V., Milovský, R., Suan, G., Mattioli, E., Pittet, B., Eisenhauer, A., 2020. Ocean acidification during the early Toarcian extinction event: evidence from boron isotopes in brachiopods. Geology 48 (12), 1184–1188. https://doi.org/10.1130/G47781.1.
Neal, C.R., Coffin, M.F., Arndt, N.T., Duncan, R.A., Eldholm, O., Erba, E., Farnetani, C., Fitton, J.G., Ingle, S.P., Ohkouchi, N., Rampino, M.R., Reichow, M.K., Self, S., Tatsumi, Y., 2008. Investigating large igneous province formation and associated paleoenvironmental events: a white paper for scientific drilling. Sci. Drill. 6, 4–18.
Nederbragt, A.J., Fiorentino, A., 1999. Stratigraphy and palaeoceanography of the Cenomanian–Turonian Boundary Event in Oued Mellegue, north-western Tunisia. Cretac. Res. 20, 47–62.
Neumann, M., Schroeder, R., 1985. Les grands foraminifères du Crétacé moyen de la région méditerranéenne. Geobios, Mémoire Special 7, 160.
Newell, N.D., 1965. Classification of the Bivalvia. Am. Mus. Novit. 2206, 1–25.
O'Brien, C.L., Robinson, S.A., Pancost, R.D., Sinninghe Damsté, J.S., Schouten, S., Lunt, D.J., Alsenz, H., Bornemann, A., Bottini, C., Brassell, S.C., Farnsworth, A., Forster, A., Huber, B.T., Inglis, G.N., Jenkyns, H.C., Linnert, C., Littler, K., Markwick, P., McAnena, A., Mutterlose, J., Naafs, D.A., Püttmann, W., Sluijs, A., van Helmond, N., Vellekoop, J., Wagner, T., Wrobel, N.E., 2017. Cretaceous sea-surface temperature evolution: constraints from TEX_{86} and planktonic foraminiferal oxygen isotopes. Earth-Sci. Rev. 172, 224–247. https://doi.org/10.1016/j.earscirev.2017.07.012.
O'Connor, L.K., Jenkyns, H.C., Robinson, S.A., Remmelzwaal, S.R., Batenburg, S.J., Parkinson, I.J., Gale, A.S., 2020. A re-evaluation of the Plenus Cold Event, and the links between CO_2, temperature, and seawater chemistry during OAE 2. Paleoceanogr. Paleoclimatol. 35, e2019PA003631. https://doi.org/10.1029/2019PA003631.
Ouikene, K., Desmares, D., Gardin, S., Benkherouf-Kechid, F., Bardin, J., 2022. Biostratigraphic and chemostratigraphic record of the Cenomanian-Turonian boundary interval of the Tellian Atlas (Algeria). Cretac. Res. 138, 105264.
Özer, S., Ahmad, F., 2016. *Caprinula* and *Sauvagesia* rudist faunas (Bivalvia) from the Cenomanian of NW Jordan. Stratigraphy and taxonomy. Cretac. Res. 58, 141–159.
Pancost, R.D., Crawford, N., Magness, S., Turner, A., Jenkyns, H.C., Maxwell, J.R., 2004. Further evidence for the development of photic-zone euxinic conditions during Mesozoic oceanic anoxic events. J. Geol. Soc. Lond. 161 (3), 353–364.
Parente, M., Frijia, G., Di Lucia, M., Jenkyns, H.C., Woodfine, R.G., Baroncini, F., 2008. Stepwise extinction of larger foraminifers at the Cenomanian/Turonian: a shallow-water perspective on nutrient fluctuations during Oceanic Anoxic Event 2 (Bonarelli Event). Geology 39, 715–718.
Paul, C.R.C., Lamolda, M.A., Mitchell, S.F., Vaziri, M.R., Gorostidi, A., Marshall, J.D., 1999. The Cenomanian–Turonian boundary at Eastbourne (Sussex, UK): a proposed European reference section. Palaeogeogr. Palaeoclimatol. Palaeoecol. 150, 83–121.
Pearce, M.A., Jarvis, I., Tocher, B.A., 2009. The Cenomanian–Turonian boundary event, OAE2 and palaeoenvironmental change in epicontinental seas: new insights from the dinocyst and geochemical records. Palaeogeogr. Palaeoclimatol. Palaeoecol. 280, 207–234.
Percival, L.M.E., Matsumoto, H.S., Callegaro, S., Erba, E., Kerr, A.C., Mutterlose, J., Suzuki, K., 2024. Cretaceous large Igneous Provinces: From volcanic formation to environmental catastrophes and biological crises. In: Hart, M.B., Batenburg, S.J., Huber, B.T., Price, G.D., Thibault, N., Wagreich, M., Walaszczyk, I. (Eds.), Cretaceous Project 200 Volume 1: the Cretaceous World. Geological Society, London. https://doi.org/10.1144/SP544-2023-88. Special Publications 544.
Petrizzo, M.R., Gale, A.S., 2023. Planktonic foraminifera document palaeoceanographic changes across the middle Cenomanian carbon-isotope excursion MCE 1: new evidence from the UK chalk. Geol. Mag. 160 (2), 372–392. https://doi.org/10.1017/S0016756822000991.
Petrizzo, M.R., Huber, B.T., Wilson, P.A., MacLeod, K.G., 2008a. Late Albian paleoceanography of the western tropical North Atlantic. Paleoceanography 23, PA1213. https://doi.org/10.1029/2007PA001517.

Petrizzo, M.R., Leoni, G., Speijer, R.P., De Bernardi, B., Felletti, F., 2008b. Dissolution susceptibility of some Paleogene Planktonic Foraminifera from ODP Site 1209 (Shatsky Rise, Pacific Ocean). J. Foraminifer. Res. 38 (4), 357–371.

Petrizzo, M.R., Huber, B.T., Falzoni, F., MacLeod, K.G., 2020. Changes in biogeographic distribution patterns of southern mid-to high latitude planktonic foraminifera during the Late Cretaceous hot to cool greenhouse climate transition. Cretac. Res. 115, 104547. https://doi.org/10.1016/j.cretres.2020.104547.

Petrizzo, M.R., Amaglio, G., Watkins, D.K., MacLeod, K.G., Huber, B.T., Hasegawa, T., Wolfgring, E., 2022. Biotic and paleoceanographic changes across the Late Cretaceous Oceanic Anoxic Event 2 in the southern high latitudes (IODP sites U1513 and U1516, SE Indian Ocean). Paleoceanogr. Paleoclimatol. 37, e2022PA004474. https://doi.org/10.1029/2022PA004474.

Philip, J., 1998. Biostratigraphie et paléobiogéographie des rudistes, évolution des concepts et progrès récents. Bulletin de la Société Géologique de France 169 (5), 689–708.

Philip, J., Airaud-Crumiere, C., 1991. The demise of the rudist-bearing carbonate platforms at the Cenomanian/Turonian boundary: a global control. Coral Reefs 10, 115–125. https://doi.org/10.1007/BF00571829.

Philip, J., Floquet, M., 2000. Late Cenomanian (94.7–93.5). In: Dercourt, J., Gaetani, M., Vrielynck, B., Barrier, E., Biju- Duval, B., Brunet, M.F., Cadet, J.P., Crasquin, S., Sandulescu, M. (Eds.), Atlas Peri-Tethys Palaeogeographical Maps. CCGM/CGMW, Paris, pp. 129–136.

Philip, J., Negra, M.H., Bachari, M., 2024. Upper Cenomanian caprinulid-radiolitid rudists (Bivalvia) from the Gattar Member of Jebel el Kebar (Central Tunisia): Stratigraphical implications and palaeobiogeographical relationships with coeval rudist-assemblages from carbonate platforms of the southern Tethyan margin. Cretac. Res. 153, 105713. https://doi.org/10.1016/j.cretres.2023.105713.

Pogge von Strandmann, P.A.E., Jenkyns, H.C., Woodfine, R.G., 2013. Lithium isotope evidence for enhanced weathering during Oceanic Anoxic Event 2. Nat. Geosci. 6, 668–672.

Pratt, L.M., 1985. Isotopic studies of organic matter and carbonate in rocks of the Greenhorn marine cycle. In: Pratt, L.M., Kauffman, E.G., Zelt, F.B. (Eds.), Fine-Grained Deposits and Biofacies of the Cretaceous Western Interior Seaway: Evidence of Cyclic Sedimentary Processes, Field Trip Guidebook, Society of Economic Paleontologists and Mineralogists, vol. 4, pp. 38–48.

Pratt, L.M., Threlkeld, C.N., 1984. Stratigraphic significance of $^{13}C/^{12}C$ ratios in mid-Cretaceous rocks of the Western Interior. Memoir Can. Soc. Petrol. Geol. 9, 305–312.

Pratt, L.M., Arthur, M.A., Dean, W.E., Scholle, P.A., 1993. Paleo-oceanographic cycles and events during the Late Cretaceous in the Western Interior Seaway of North America. In: Caldwell, W.G.E., Kauffman, E.G. (Eds.), Geol. Assoc. Can. Spec. Pap., vol. 39, pp. 333–353.

Prazeres, M., Roberts, T.E., Pandolfi, J.M., 2017. Variation in sensitivity of large benthic Foraminifera to the combined effects of ocean warming and local impacts. Sci. Report. 7, 45227.

Reddin, C.J., Kocsis, Á.T., Kiessling, W., 2019. Climate change and the latitudinal selectivity of ancient marine extinctions. Paleobiology 45, 70–84. https://doi.org/10.1017/pab.2018.34.

Reddin, C.J., Nätscher, P.N., Kocsis, ÁT., Pörtner, H. O., Kiessling, W., 2020. Marine clade sensitivities to climate change conform across time scales. Nat. Clim. Chang. 10, 249–253.

Robinson, S.A., Heimhofer, U., Hesselbo, S.P., Petrizzo, M.R., 2017. Mesozoic climates and oceans–a tribute to Hugh Jenkyns and Helmut Weissert. Sedimentology 64 (1), 1–15. https://doi.org/10.1111/sed.12349.

Russo, F., 2014. Calcareous nannofossil revised biostratigraphy of the latest Albian-earliest Campanian time interval (Late Cretaceous). PhD Thesis,. University of Milan, Italy.

Sageman, B.B., Meyers, S.R., Arthur, M.A., 2006. Orbital time scale and new C-isotope record for Cenomanian-Turonian boundary stratotype. Geology 34, 125–128.

Sageman, B.B., Jones, M.M., Arthur, M.A., Niezgodzki, I., Horton, D.E., 2024. Late Cenomanian Plenus event in the Western Interior Seaway. Cretac. Res. 156, 105798.

Salama, Y., Özer, S., 2019. *Durania cornupastoris* rudist from the Turonian of El-Hassana Dome (Abu Roash area), Egypt: Systematic palaeontology and palaeoecology. J. Afr. Earth Sci. 152, 128–139.

Scaife, J.D., Ruhl, M., Dickson, A.J., Mather, T.A., Jenkyns, H.C., Percival, L.M.E., Hesselbo, S.P., Cartwright, J., Eldrett, J.S., Bergman, S.C., Minisini, D., 2017. Sedimentary mercury enrichments as a marker for submarine large igneous province volcanism? Evidence from the mid-Cenomanian event and Oceanic Anoxic Event 2 (Late Cretaceous). Geochem. Geophys. Geosyst. 18 (12), 4253–4275.

Schlagintweit, F., Yazdi-Moghadam, M., 2021. *Moncharmontia* De Castro 1967, benthic foraminifera from the middle–upper Cenomanian of the Sarvak Formation of SW Iran (Zagros Zone): a CTB survivor taxon. Micropaleontology 67 (1), 19–29.

Schlanger, S.O., Jenkyns, H., 1976. Cretaceous oceanic anoxic events: causes and consequences. Geol. Mijnb. 55 (3–4), 179–184.

Schlanger, S.O., Arthur, M.A., Jenkyns, H.C., Scholle, P.A., 1987. The Cenomanian-Turonian Oceanic Anoxic Event, I. Stratigraphy and distribution of organic carbon-rich beds and the marine $\delta^{13}C$ excursion. Geol. Soc. Lond. Spec. Publ. 26, 371–399.

Schmidt, C., Heinz, P., Kucera, M., Uthicke, S., 2011. Temperature-induced stress leads to bleaching in larger benthic foraminifera hosting endosymbiotic diatoms. Limnol. Oceanogr. 56, 1587–1602.

Schmidt, C., Kucera, M., Uthicke, S., 2014. Combined effects of warming and ocean acidification on coral reef Foraminifera *Marginopora vertebralis* and *Heterostegina depressa*. Coral Reefs 33, 805–818. https://doi.org/10.1007/s00338-014-1151-4.

Scholle, P.A., Arthur, M.A., 1980. Carbon isotope fluctuations in Cretaceous pelagic limestones: potential stratigraphic and petroleum exploration tool. Am. Assoc. Pet. Geol. Bull. 64, 67–87.

Schröder-Adams, C.J., Herrle, J.O., Selby, D., Quesnel, A., Froude, G., 2019. Influence of the high Arctic igneous province on the Cenomanian/Turonian boundary interval, Sverdrup Basin, High Canadian Arctic. Earth Planet. Sci. Lett. 511, 76–88.

Scotese, C.R., 2016. PALEOMAP PaleoAtlas for GPlates and the PaleoData Plotter Program, PALEOMAP Project. http://www.earthbyte.org/paleomap-paleoatlas-for-gplates/.

Sepkoski Jr., J.J., 1996. Patterns of Phanerozoic extinction: A perspective from global data base. In: Walliser, O.H. (Ed.), Global Events and Event Stratigraphy in the Phanerozoic: Results of the International Interdisciplinary Cooperation in the IGCP-Project 216 Global Biological Events in Earth History. Springer, Berlin Heidelberg, pp. 35–51.

Simmons, M., Bidgood, M., 2023. "Larger" Benthic Foraminifera of the Cenomanian. A review of the identity and the stratigraphic and palaeogeographic distribution of non-fusiform planispiral (or near-planispiral) forms. Acta Palaeontol. Romaniae 19 (2), 39–169. https://doi.org/10.35463/j.apr.2023.02.06.

Sinninghe Damsté, J.S., van Bentum, E.C., Reichart, G.J., Pross, J., Schouten, S., 2010. A CO_2 decrease-driven cooling and increased latitudinal temperature gradient during the mid-Cretaceous Oceanic Anoxic Event 2. Earth Planet. Sci. Lett. 293, 97–103.

Skelton, P.W., 2003. The operation of the major geological carbon sinks. In: Skelton, P. W., Spicer, R.A., Kelley, S.P., Gilmour, I. (Eds.), The Cretaceous World. Cambridge University Press, Cambridge, England, pp. 259–266.

Solak, C., Tasli, K., Koç, H., 2020. An Albian-Turonian shallow-marine carbonate succession of the Bey Daglari (Western Taurides, Turkey): biostratigraphy and a new benthic foraminifera *Fleuryana gediki* sp. nov. Cretac. Res. 108, 104321. https://doi.org/10.1016/j.cretres.2019.104321.

Song, H., Kemp, D.B., Tian, L., Chu, D., Song, H., Dai, X., 2021. Thresholds of temperature change for mass extinctions. Nat. Commun. 12, 4694. https://doi.org/10.1038/s41467-021-25019-2.

Steuber, T., 1999. Cretaceous rudists of Boeotia, Central Greece. Spec. Pap. Palaeontol. 61, 1–229.

Steuber, T., Löser, H., 2000. Species richness and abundance patterns of Tethyan Cretaceous rudist bivalves (Mollusca: Hippuritacea) in the Central-Eastern Mediterranean and Middle East, analysed from a palaeontological data base. Palaeogeogr. Palaeoclimatol. Palaeoecol. 162, 75–104. https://doi.org/10.1016/S0031-0182(00)00106-1.

Steuber, T., Scott, R.W., Mitchell, S.F., Skelton, P.W., 2016. Stratigraphy and diversity dynamics of Jurassic-Cretaceous Hippuritida (rudist bivalves). In: Treatise on Invertebrate Paleontology Online, no. 81, Part N, Revised, Volume 1, Chapter 26C. University of Kansas, Lawrence, pp. 1–17.

Steuber, T., Löser, H., Mutterlose, J., Parente, M., 2023. Biogeodynamics of Cretaceous marine carbonate production. Earth Sci. Rev. 238, 104341. https://doi.org/10.1016/j.earscirev.2023.104341.

Trabucho Alexandre, J., Tuenter, E., Henstra, G.A., van der Zwan, K.J., van de Wal, R.S., Dijkstra, H.A., de Boer, P.L., 2010. The mid-Cretaceous North Atlantic nutrient trap: black shales and OAEs. Paleoceanography 25, PA4201. https://doi.org/10.1029/2010PA001925.

Trudgill, M., Rae, J., Crumpton-Banks, J., van Mourik, M., Adloff, M., Burke, A., Corsetti, F., Doherty, D., Greenop, R., Hong, W.-L., Lepland, A., McIntyre, A., Neiroukh, N., Rose, C., Ruhl, M., Saunders, D., Stüeken, E., West, J., Whiteford, R., Greene, S., 2021. Pulses of ocean acidification at the Triassic-Jurassic boundary recorded by boron isotopes. Goldschmidt 2021 Abstr. https://doi.org/10.7185/gold2021.6335.

Tsikos, H., Jenkyns, H.C., Walsworth-Bell, B., Petrizzo, M.R., Forster, A., Kolonic, S., Erba, E., Premoli Silva, I., Baas, M., Wagner, T., Sinninghe Damsté, J.S., 2004. Carbon-isotope stratigraphy recorded by the Cenomanian–Turonian Oceanic Anoxic Event: Correlation and implications based on three localities. J. Geol. Soc. Lond. 161, 711–719.

Turgeon, S.C., Creaser, R.A., 2008. Cretaceous Oceanic Anoxic Event 2 triggered by a massive magmatic episode. Nature 454, 323–326. https://doi.org/10.1038/nature07076.

van Bentum, E.C., Reichart, G.J., Forster, A., Sinninghe Damsté, J.S., 2012. Latitudinal differences in the amplitude of the OAE-2 carbon isotopic excursion: pCO_2 and paleoproductivity. Biogeosciences 9 (2), 717–731.

van Helmond, N.A.G.M., Sluijs, A., Reichart, G.J., Sinninghe Damsté, J.S., Slomp, C.P., Brinkhuis, H., 2014. A perturbed hydrological cycle during Oceanic Anoxic Event 2. Geology 42, 123–126.

van Helmond, N.A.G.M., Sluijs, A., Papadomanolaki, N., Plint, A.G., Gröcke, D., Pearce, M.A., Eldrett, J.S., Trabucho-Alexandre, J., Walaszczyk, I., van de Schootbrugge, B., Brinkhuis, H., 2016. Equatorward phytoplankton migration during a cold spell within the Late Cretaceous super-greenhouse. Biogeosciences 13, 2859–2872.

Voigt, S., Gale, A.S., Flögel, S., 2004. Midlatitude shelf seas in the Cenomanian–Turonian greenhouse world: Temperature evolution and North Atlantic circulation. Paleoceanography 19, PA4020. https://doi.org/10.1029/2004PA001015.

Voigt, S., Gale, A.S., Voigt, T., 2006. Sea-level change, carbon cycling and palaeoclimate during the late Cenomanian of Northwest Europe; an integrated palaeoenvironmental analysis. Cretac. Res. 27, 836–858.

Voigt, S., Aurag, A., Leis, F., Kaplan, U., 2007. Late Cenomanian to middle Turonian high-resolution carbon isotope stratigraphy: New data from the Münsterland Cretaceous Basin, Germany. Earth Planet. Sci. Lett. 253, 196–210.

Voigt, S., Erbacher, J., Mutterlose, J., Weiss, W., Westerhold, T., Wiese, F., Wilmsen, M., Wonik, T., 2008. The Cenomanian-Turonian of the Wunstorf section (North Germany): global stratigraphic reference section and new orbital time scale for Oceanic Anoxic Event 2. Newsl. Stratigr. 43, 65–89. https://doi.org/10.1127/0078-0421/2008/0043-0065.

Watkins, D.K., 1985. Biostratigraphy and paleoecology of calcareous nannofossils in the Greenhorn Marine Cycle. In: Pratt, L.M., Kauffman, E.G., Zelt, F.B. (Eds.), Fine-Grained Deposits and Biofacies of the Cretaceous Western Interior Seaway: Evidence of Cyclic Sedimentary Processes, 4. Society of Economic Paleontologists and Mineralogists, Field Trip Guidebook, Tulsa, pp. 151–156.

Wendler, I., 2013. A critical evaluation of carbon isotope stratigraphy and biostratigraphic implications for Late Cretaceous global correlation. Earth Sci. Rev. 126, 116–146.

West, O.L., Leckie, R.M., Schmidt, M., 1998. Foraminiferal paleoecology and paleoceanography of the Greenhorn cycle along the southwestern margin of the Western Interior Sea. SEPM, Concepts Sedimentol. Paleontol. 6, 79–99.

Wilson, P.A., Norris, R.D., Cooper, M.J., 2002. Testing the Cretaceous greenhouse hypothesis using glassy foraminiferal calcite from the core of the Turonian tropics on Demerara rise. Geology 30 (7), 607–610.

Zeebe, R.E., 2001. Seawater pH and isotopic paleotemperatures of Cretaceous oceans. Palaeogeogr. Palaeoclimatol. Palaeoecol. 170, 49–57. https://doi.org/10.1016/S0031-0182(01)00226-7.

Zheng, X.Y., Jenkyns, H.C., Gale, A.S., Ward, D.J., Henderson, G.M., 2013. Changing ocean circulation and hydrothermal inputs during Ocean Anoxic Event 2 (Cenomanian–Turonian): evidence from Nd-isotopes in the European shelf sea. Earth Planet. Sci. Lett. 375, 338–348.